

11-2017

Analytical and Numerical Approaches on the Stiffness of Magnetorheological Fluid Filled Spring

Stanislav Sikulskyi

Follow this and additional works at: <https://commons.erau.edu/edt>



Part of the [Aerospace Engineering Commons](#)

Scholarly Commons Citation

Sikulskyi, Stanislav, "Analytical and Numerical Approaches on the Stiffness of Magnetorheological Fluid Filled Spring" (2017).
Dissertations and Theses. 375.
<https://commons.erau.edu/edt/375>

This Thesis - Open Access is brought to you for free and open access by Scholarly Commons. It has been accepted for inclusion in Dissertations and Theses by an authorized administrator of Scholarly Commons. For more information, please contact commons@erau.edu, wolfe309@erau.edu.

ANALYTICAL AND NUMERICAL APPROACHES ON THE STIFFNESS
OF MAGNETORHEOLOGICAL FLUID FILLED SPRING

A Thesis

Submitted to the Faculty

of

Embry-Riddle Aeronautical University

by

Stanislav Sikulskyi

In Partial Fulfillment of the

Requirements for the Degree

of

Master of Science in Aerospace Engineering

November 2017

Embry-Riddle Aeronautical University

Daytona Beach, Florida

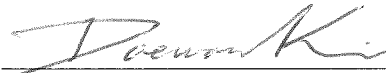
ANALYTICAL AND NUMERICAL APPROACHES ON THE STIFFNESS
OF MAGNETORHEOLOGICAL FLUID FILLED SPRING

by

Stanislav Sikulskyi

A Thesis prepared under the direction of the candidate's committee chairman,
Dr. Daewon Kim, Department of Aerospace Engineering, and has been approved by the
members of the thesis committee. It was submitted to the School of Graduate Studies and
Research and was accepted in partial fulfillment of the requirements for the degree of
Master of Science in Aerospace Engineering.

THESIS COMMITTEE



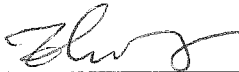
Chairman, Dr. Daewon Kim



Member, Dr. Sirish Namilae



Member, Dr. Dongeun Seo



Member, Dr. Feng Zhu



Graduate Program Coordinator, Dr. Magdy Attia

12.7.2017

Date



Dean of College of Engineering, Dr. Maj Mirmirani

12/7/2017

Date



Vice Chancellor, Academic Support, Dr. Christopher Grant

12/7/17

Date

ACKNOWLEDGMENTS

I would like to thank my thesis advisor Dr. Daewon Kim for introducing me to the field of Smart Materials and supporting me greatly at every step of pursuing the Master of Science degree in Aerospace Engineering.

I recognize the committee members, Dr. Sirish Namilae, Dr. Dongeun Seo, and Dr. Feng Zhu, for their suggestions in improvement the research. I also would like to acknowledge Embry-Riddle Aeronautical University for providing high quality education, faculty support, equipment and facilities to perform the research, and the great experience of being Graduate Teaching and Research Assistant.

Finally, I would like to thank my parents for all the support they provided me over the years and being my first and main teachers.

TABLE OF CONTENTS

LIST OF TABLES	v
LIST OF FIGURES	vi
SYMBOLS.....	viii
ABBREVIATIONS	x
ABSTRACT.....	xi
1. Introduction	1
1.1. Passive, active and semi-active methods	4
1.1.1. Varied and Variable Stiffness Devices.....	7
1.2. MR Fluid.....	9
1.2.1. MR fluid models	11
1.2.2. MR fluid modes	15
1.2.3. MR fluid devices.....	17
2. Objective and Approaches	25
3. Analytical Approach	26
3.1. Spring mechanics	26
3.2. Analytical approach for MR fluid	31
4. Results of Analytical Approach	38
5. Numerical Approach	44
5.1. Steady-state simulation	44
5.2. Transient simulation.....	47
6. Conclusion.....	49
REFERENCES	50

LIST OF TABLES

Table 4.1 Magnetic field (flux density) dependent values of yield stress and shear moduli (Laun et al, 2010).....	42
Table 5.1 Geometry of the helical hollow spring	45
Table 5.2 Mesh quality in ANSYS Mechanical and CFX (Steady-state simulation).....	46

LIST OF FIGURES

Figure 1.1 Structural failure due to wind induced vibrations of (a) the Taiwan Power Co wind turbine blade (Chiu & Hsu, 2013) and (b) Tacoma bridge (Ohanian & Markert, 2007)	1
Figure 1.2 Collapsed section of the Hanshin Expressway during the Hyogoken-Nanbu Earthquake (Akai et al., 1995)	2
Figure 1.3 Lost rudder due to flutter effect and prior structural deviation	3
Figure 1.4 Rubber support in (a) engine mount system, (b) a bridge bearing	4
Figure 1.5 (a) Stack and (b) flat configurations of PZT to control wing vibrations	6
Figure 1.6 Schematic models of varied (a) stiffness and (b) damping dampers	8
Figure 1.7 Configuration of varied stiffness/damping damper (Xu et al., 2016).....	9
Figure 1.8 MR fluid in passive and active states (Choi & Han, 2013)	10
Figure 1.9 Comparison of Newtonian, Bingham, and Herschel-Bulkley models	11
Figure 1.10 Biviscous model	13
Figure 1.11 MR fluid (a) flow, (b) shear and (c) squeeze modes (Spaggiari, 2013)	15
Figure 1.12 Flow and shear combination mode MR damper (Wang & Meng, 2001).....	16
Figure 1.13 (a)-(d) MR dampers configurations (Spaggiari, 2013; Poynor, 2001, Zhu et al., 2012)	18
Figure 1.14 Configuration of and manufactured MR mixed-mode mount (Choi et al., 2008)	20
Figure 1.15 BWI Group MR mount for car powertrain (BWI)	20
Figure 1.16 MR (a) brake and (b) clutch common configurations and commercial devices of LORD Corporation (Carlson et al., 2007; LORD, 2011)	21
Figure 3.1 Geometry of a helical hollow spring with annular cross section.....	25
Figure 3.2 Stiffness components of the spring with change of a spring (a) index ($\alpha=10^\circ, d=10$ mm), (b) pitch angle ($i=8$ – spring index, $d=10$ mm).....	29
Figure 3.3 Linear flow between two concentric rotating cylinders	33
Figure 3.4 Velocity profile (mm/s) for transient flow in the spring cross section at the moment of: (a) 0.2% spring elongation or $t=0.001$ s; (b) 4% spring elongation or $t=0.02$ s ($f=1$ Hz, $t=1/2f=0.5$ s, $\delta=10.75$ mm, deflection rate $=\delta/t=21.5$ mm/s, $r^*=0.25d_i$, $d_i=7$ mm, $R=17.5$ mm, $n=4$).....	33
Figure 3.5 MR fluid stiffness portion $k_{(MR\ fluid)}$ with change of relative deflection δ^- and loading frequency f ($d_{ext}=8$ mm, $i=4.375$, $\xi=0.875$, $\alpha=5.3^\circ$, $n=4$, $B\approx 0.14$ Ts, $G^*=3.35$ MPa, $\tau_y=6.6$ kPa).....	36
Figure 3.6 Viscous portion of MR fluid stiffness for different spring designs ($f=20$ Hz, $\delta^-=0.5$, $d_{ext}=8$ mm, $\xi=0.875$, $n=4$, $B\approx 0.14$ Ts, $G^*=3.35$ MPa, $\tau_y=6.6$ kPa)	36

LIST OF FIGURES

Figure 4.1 Force – deflection relation of the MR fluid filled spring obtained in the present study.....	38
Figure 4.2 Stiffness of the hollow spring and MR fluid for different: (a) spring index ($G=0.1$ GPa, $\alpha=5^\circ$, $\xi=0.9$), (b) pitch angle ($G=0.1$ GPa, $\xi=0.9$, $i=6$), (c) void ratio ($G=0.1$ GPa, $\alpha=5^\circ$, $i=6$), (d) shear modulus of the hollow spring material ($i=6$, $\alpha=5^\circ$, $\xi=0.9$).....	40
Figure 4.3 Performance of close-to-optimum MR fluid filled spring design ($G = 0.5$ GPa, $\xi = 0.875$, $\alpha = 5^\circ$, $i = 4.5$).....	43
Figure 5.1 Coupling of numerical solver in 2-way steady-state simulation	45
Figure 5.2 Meshes in (a) ANSYS Mechanical and (b) CFX	46
Figure 5.3 Steady-state (a) ANSYS Mechanical and (b) FSI solutions for the deflection of the MR fluid and hollow spring.....	46
Figure 5.4 Transient (a) ANSYS Mechanical and (b) FSI solutions for the deflection of the MR fluid and hollow spring.....	48

SYMBOLS

D	spring mean diameter
p	spring pitch
α	spring pitch angle
h	length of the spring
n	number of coils of the spring
d_i	inner radius of the annular cross section
d_o	outer radius of the annular cross section
i	spring index
ξ	void ratio of the annular cross section
k	overall stiffness of the spring
G	shear modulus of the spring material
J_p	polar moment of inertia of the annular cross section
R	mean radius of the spring
γ	torsional rigidity of the spring coil
β	flexural rigidity of the spring coil
S	sine function of the spring pitch angle
C	cosine function of the spring pitch angle
δ	overall spring deflection
R_0	initial spring coil radius
C_0	cosine function of the initial spring pitch angle
S_0	sine function of the initial spring pitch angle
δ_{T_b}	deflection component of shearing force
δ_{T_t}	deflection component of axial force
δ_{M_b}	deflection component of bending moment
δ_{M_t}	deflection component of torsional moment
C_b	shearing rigidity of the spring coil
C_t	axial rigidity of the spring coil
D_b	bending rigidity of the spring coil
D_t	torsional rigidity of the spring coil
k_n	shear correction factor
ν	Poisson's ratio
τ	shear stress
τ_y	yield shear stress
$\dot{\gamma}$	shear strain rate
η	post-yield plastic viscosity
G^*	complex shear modulus
G'	storage shear modulus
G''	loss shear modulus
K	consistency index
n'	flow behavior index

B	magnetic field induction
τ_{yd}	dynamic yield stress
η_{po}	post-yield viscosity
τ_{ys}	static yield stress
η_{pr}	pre-yield viscosity
η_{∞}	viscosity at infinite shear strain rate
$k_{MRF}^{pre-yield}$	pre-yield portion of MR fluid stiffness
i_{MRF}	index of the MR fluid spring
r^*	radius of the MR fluid solid core
J_p^*	polar moment of inertia of the MR fluid solid core
f	frequency of the applied load
φ	angle of twist of the spring coil
$\bar{\delta}$	relative deflection of the spring
h_0	initial length of the spring
γ_y	shear strain corresponding to the shear yield stress
r_i	inner radius of the annular cross section
V	velocity distribution in the flow
t	time
μ	viscosity
V_{max}	maximum speed of the flow
y	radial coordinate
M	resistance moment of the post-yield MR fluid
$F_{MRF}^{post-yield}$	post yield force of MR fluid
w	rotational velocity
$k_{MRF}^{post-yield}$	post-yield portion of MR fluid stiffness
k_{MRF}	total MR fluid stiffness
μ_r	magnetic permeability

ABBREVIATIONS

MR	magnetorheological
FSI	fluid-structural interaction
FAR	Federal Aviation Regulations
AMD	active mass damper
ATS	active tendon system
TMD	tuned mass damper
PZT	lead zirconate titanate
VSD	variable stiffness device
ER	electrorheological
TFD	tactile feedback device

ABSTRACT

Sikulskiy, Stanislav MSAE, Embry-Riddle Aeronautical University, November 2017.
Analytical and Numerical Approaches on the Stiffness of MR Fluid Filled Spring.

A solid mechanical spring generally exhibits uniform stiffness. This thesis studies a mechanical spring filled with magnetorheological (MR) fluid to achieve controllable stiffness. The hollow spring filled with MR fluid is subjected to a controlled magnetic field in order to change the viscosity of the MR fluid and thereby to change the overall stiffness of the spring. MR fluid is considered as a Bingham viscoplastic linear material in the mathematical model. The goal of this research is to study the feasibility of such spring system by analytically and numerically computing the effects of MR fluid on the overall spring stiffness. For this purpose, spring mechanics and MR fluid behavior are studied to increase the accuracy of the analytical analysis. Numerical simulations are also performed to generate some assumptions, which simplify calculations in the analytical part of the analysis. The accuracy of the present analytical approach is validated by comparing the results to previously known experimental results. Overall stiffness variations of the spring, calculated through the developed equations, are also discussed for different spring designs. Simulation of a helical hollow spring with an annular cross section filled with MR fluid is performed using ANSYS by means of two-way Fluid-Structural Interaction (FSI). The simulation shows that MR fluid effect is capable of controlling the stiffness of the spring in some ranges.

1. Introduction

Due to rapid technological developments in the last century, structural components implemented in aerospace, mechanical, civil, and other engineering fields have obtained dimensional and mechanical advantages, such as being lighter or having higher strength with smaller principal dimensions. This is probably owing to the development of new materials, manufacturing innovations, and advanced design techniques. Regardless of these developments, there are still some technical challenges present in man-made structures during their operations, such as structural instability due to vibration. Controlling vibration or increasing dynamic stability of a structure is of crucial importance because it can lead the structure to its limit state or even failure at much lower loads than it was designed for. There are many well known cases when bridges, buildings, towers, and other structures were damaged or completely destroyed by vibrations, particularly resonance, induced by either wind or earthquake (Wang et al., 2014). Some of these cases are shown in Figure 1.1 and Figure 1.2.

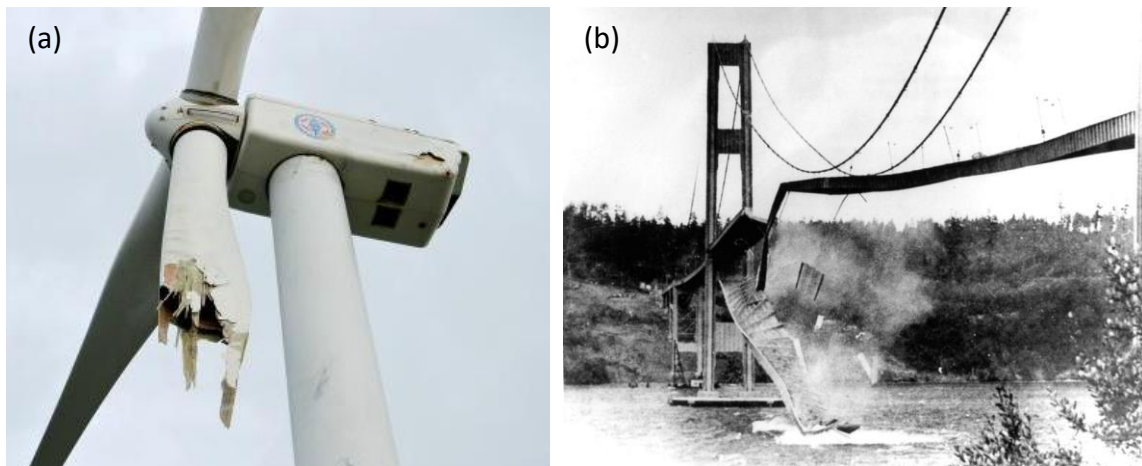


Figure 1.1 Structural failure due to wind induced vibrations of (a) the Taiwan Power Co wind turbine blade (Chiu & Hsu, 2013) and (b) Tacoma bridge (Ohanian & Markert, 2007).



Figure 1.2 Collapsed section of the Hanshin Expressway during the Hyogoken-Nanbu Earthquake (Akai et al., 1995).

In the aerospace industry, structural elements are even more susceptible to vibrations. Additionally, wings, blades, stabilizing and control surfaces can be subjected to aeroelastic effects and vibrations generated by aircraft dynamic modes. Having achieved the satisfactory static strength, first aircrafts and especially rotorcrafts still used to be a precarious mean of transportation. Lots of vehicles failed due to the dynamic loads before sufficient reliability was reached (Hodges and Pierce, 2011). Considering the potential danger of vibrations, their analysis and test have become a standard part of a structural design procedures in aerospace, civil, marine engineering, etc. (Richardson and Ramsey, 1981). For example, all civil transport aircraft manufactured in the US must be designed, built, and tested according to the Federal Aviation Regulations (FAR), Part 25 - Airworthiness Standards: Transport Category Airplanes, where in Section 25.629 all the aeroelastic stability requirements are stated (FAA, 1965). Nowadays, vibrations are controlled much better than used to be and sufficiently precise enough not to cause complete failure in most of cases. This better controllability, in addition to fatigue failure studies, allows in decreasing the design-limit load factor, i.e. reduce the weight of parts

and components, and extend a fatigue life of structures (Grover, 1966). Nevertheless, when some kinds of operational deviations are present in the main structural components, an effect of vibration can be more severe. For instance on March 6, 2005, the Airbus A310-308 of Air Transat airline (Flight 961) completely lost its rudder after it was affected by the Dutch roll and flutter, and some prior structural defect as determined through the investigation (Transportation Safety Board of Canada, 2007). The consequence of the event was captured after the emergency landing, which is shown in Figure 1.3.

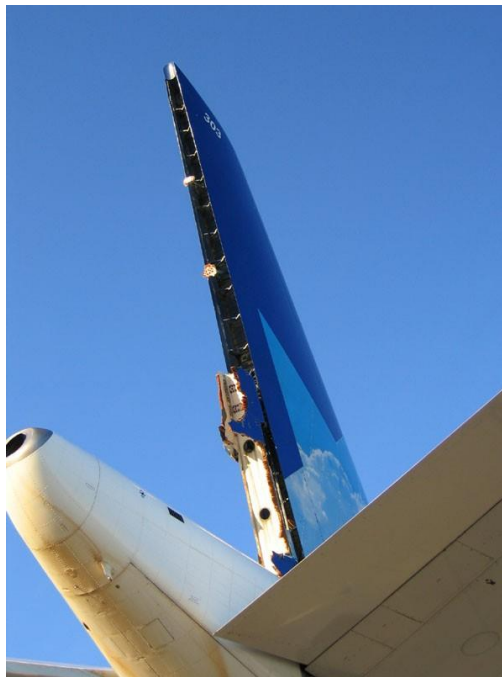


Figure 1.3 Lost rudder due to flutter effect and prior structural deviation.

For the last decades, several approaches to reduce and control vibrations were developed with great success. Nonetheless, new tasks and higher requirements arise as a result of intensive technology development, strong demand of lighter structures, and requirements of thinner and more flexible structures. Hence, the dynamic stability of aforementioned structures stays as an important task to be solved and much more improved in various fields of engineering.

1.1. Passive, active and semi-active methods of vibration control

In general, the techniques developed to control vibration by providing stability to structure can be divided into three groups: passive, active, and semi-active methods (Preumont, 2011).

The passive method can be implemented by designing a structure using materials with appropriate dynamic stability properties (i.e. thermally stable, energy absorbing property, etc.) or devices that work without external control (rubber damper, any mechanical or hydraulic damper) (Zhu et al., 2012). Thermally stable materials are used to maintain mechanical properties of the structures unchanged in a wide range of operational temperatures. This is important in case of designing internal combustion or jet engines, some parts of engine mount systems, supersonic aircraft external panels, etc. Rubber damper, shown in Figure 1.4, is the most common vibration control device used in every engineering related field, e.g. heavy industrial equipment, supports for buildings, bridges and other civil structures, engine mounts in cars, aircrafts, etc (Shmyrov et al., 2010).

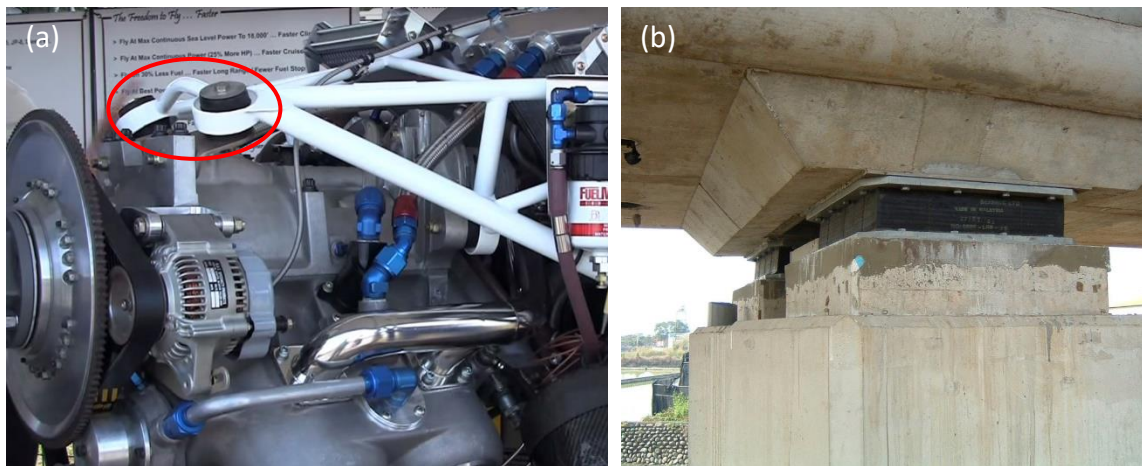


Figure 1.4 Rubber support in (a) engine mount system, (b) a bridge bearing

Passive vibration control method is used in the majority of applications due to its simplicity and the low cost. However, some major drawbacks of this approach, such as

constant dynamic response and relatively large weight, limit its application in cases of more complex, dynamically changing vibration profiles.

The active method uses a system that consists of actuators and sensors that are connected to a target structure as well as a control system. Based on sensors' feedback, the control system activates the actuators to stabilize the structure. Occasionally, some active damping systems can be lighter and even cheaper comparing to the passive system with the same effectiveness (Preumont, 2011). First researches on active method appeared in the 1950s, however, it started to be implemented practically around 1990s (Xu et al., 2016). Such a delay in the implementation of the method can be explained by the need of developed control systems and advanced manufacturing technologies, which appeared at the end of the last century. Nowadays, active damping method is used in some manufacturing processes where absolute vibration-free environment is required, example of which is the production of semiconductor wafers during photolithography. In civil engineering the most common applications of active method are active mass damper (AMD) and active tendon system (ATS), which are used to provide dynamic stability to high-rise buildings and other structures (Xu et al., 2016). In some cases, active vibration control devices are obtained simply by replacing a constant stiffness elements, i.e. springs, in existing passive damping systems with the actuators, and adding the corresponding control system. This can be applied to AMD, which was obtained by adding an actuator to the tuned mass damper (TMD). While the only problem with control system is its complexity, transition from passive to active method also requires an actuator to have a minimum weight for a needed load capacity, respond quickly to external stimuli and to be easily controlled. For that purpose, smart materials are mostly used as actuators.

Piezoelectric materials, particularly lead zirconate titanate (PZT), became the most popular choice for actuators. Being stiff and providing large actuating force for comparably small size and weight, PZT based damping systems are intensively studied to be implemented in aerospace industry. Stacked PZTs (Ardelean et al., 2006) and flat PZT (Prakash et al., 2009) actuators are studied to be used for vibration/flutter control of a wing and control surfaces of an aircraft, and can be seen in Figure 1.5.

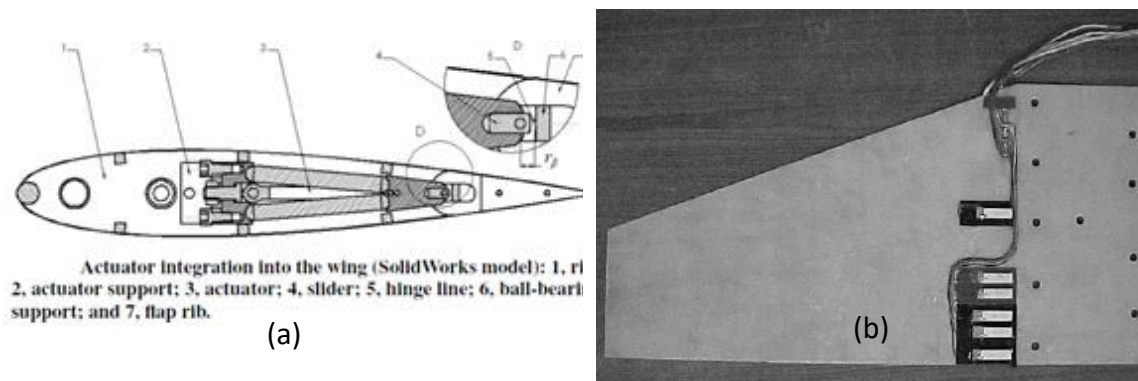


Figure 1.5 (a) Stacked (Ardelean et al., 2006) and (b) flat (Prakash et al., 2009) configurations of PZT to control wing vibrations.

Although purely active control is not used widely yet, smart materials are being intensively developed making the active method a promising technique to improve a dynamic stability of structures.

Lastly, the semi-active method is essentially passive and cannot input energy into the structure to stabilize the structural system like it is done in the active method. The semi-active devices generally change their damping properties enabling control of structural vibrations. Meanwhile, this method should be distinguished from the hybrid damping systems, particularly hybrid mass damper (HMD), which represents a combination of passive and active devices coupled in one damping system (Chu et al., 2005).

Apparently, the primary property that is controlled in semi-active method is stiffness of the damping system, which can be shown as:

$$k = k_0 + k_v \quad (1)$$

where k – is the overall stiffness of a damping system, k_0 – constant portion of the stiffness provided by passive damping effect, and k_v – variable (controlled) portion of the stiffness due to embedded active control.

The main advantages of this type of control over active method are that it usually requires much less energy to be operated, as the energy is used to change only the variable portion of the stiffness k_v , and simplifies the overall system as it often uses modest control systems (Preumont, 2011). If the variable portion of the stiffness is partially or completely lost due to some improper work of a control system, the damping device retains its constant stiffness portion. Often enough, passive stiffness k_0 might be sufficient to prevent complete failure of the structure. Owing to the abovementioned advantages of the semi-active vibration control method, variable stiffness devices (VSDs) obtained significant number of applications, especially in civil Engineering (Xu et al., 2016) and automotive industry (Choi & Han, 2016).

1.1.1. Varied and Variable Stiffness Devices

First VSDs were proposed around 1920s, long before active vibration method appeared, and did not utilize smart materials to create a variable portion of the stiffness k_v . They were designed by simply introducing an additional controlled damping element into the passive system. These devices are divided into two groups: varied stiffness dampers and varied damping dampers, schematic models of which can be represented as in Figure 1.6. It can be seen that the behavior of the devices is similar with the only difference that in the first case the additional damping element has only two extreme positions, while the second type of the element possesses an ability to change its damping properties within a

certain range. A typical hydraulic damper, shown in Figure 1.7, can be related to both of these damping devices groups depending on a type of valve installed in the system (Xu et al., 2016).

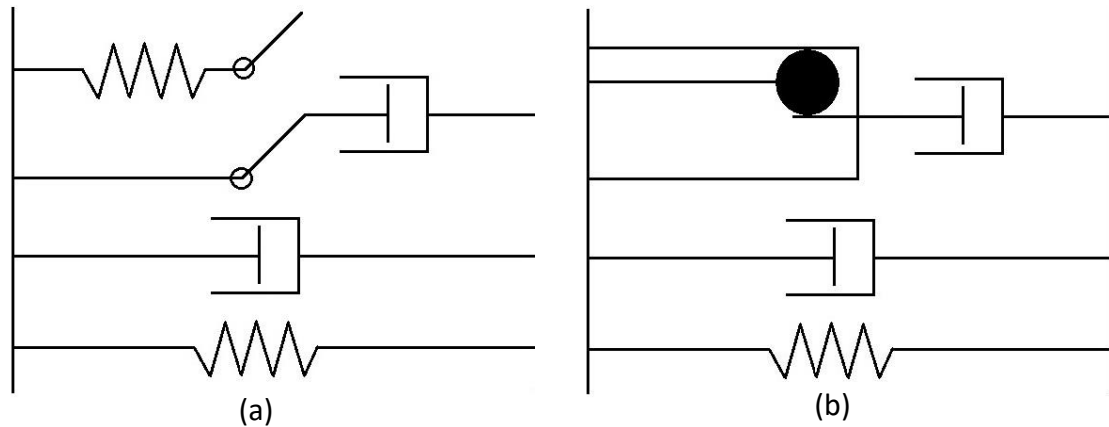


Figure 1.6 Schematic models of varied (a) stiffness and (b) damping dampers.

In the Figure 1.7, the additional element is represented with the second channel and a valve. If the valve has only two extreme positions with different flow coefficients, then such a device is considered to be varied stiffness damper. Due to its limited performance, such type of damper is used mostly to avoid the natural frequency of the target structure. On the contrary, if the valve can be controlled, e.g. with a servo, and change its flow coefficient gradually within a given range, then such a device is called variable damping device. In this case, its damping force can be precisely adjusted to withstand dynamically changing vibrations.

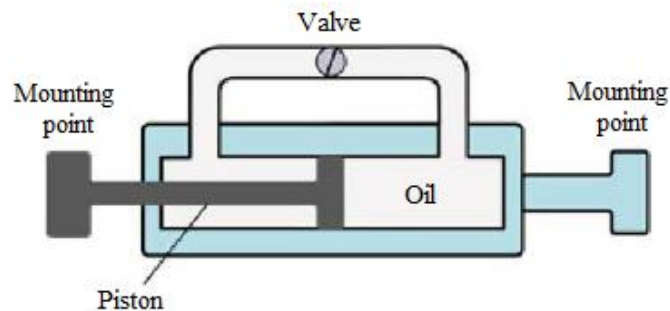


Figure 1.7 Configuration of varied stiffness/damping damper (Xu et al., 2016)

Embedding smart materials technology to the semi-active control allowed to significantly improve the damping properties of the systems and to simplify the structure of such devices. Such smart materials as piezoelectric ceramics (Xu et al., 2016), shape memory alloys (Damanpack et al., 2014), electrorheological (ER) fluids (Onoda et al., 1997), and other materials are studied for vibration control application. Within these materials ER fluid obtained the largest interest due to its controllable viscosity and quick response time. However, with the advent of stable magnetorheological (MR) fluid, the research focus moved from ER to MR fluid, as the latter one has much higher viscosity, i.e. damping potential.

1.2 MR Fluid

MR fluid is considered to be invented in late 1940s by Jacob Rabinow at the US National Bureau of Standards. In the late 1940s and early 1950s, there were more publications and patents pertinent to MR fluid technology rather than ER fluid, the latter smart fluid obtained a bigger interest for the next four decades. Despite the higher damping performance of MR fluid, obtaining a stable form of the fluid appeared to be a serious problem. After this issue was solved by introducing special additives to the fluid to reduce sedimentation of the ferromagnetic particles, MR fluid attracted attention in terms of research and some devices based on its technology found their commercial applications (Jolly et al., 1999).

MR fluid represents a type of smart material, which in essence is a suspension of magnetically responsive particles in a liquid carrier, usually oil. Small amounts of different additional components are added by manufacturers not only to stabilize the suspension, but also to improve its viscous and dynamic properties. When subjected to a magnetic field,

the responsive particles build chains and significantly increase the viscosity of the MR fluid, like it is shown in Figure 1.8. This change in properties of the fluid can be controlled by varying the magnetic field strength, and thus, allows the usage of MR fluid in semi-active control.

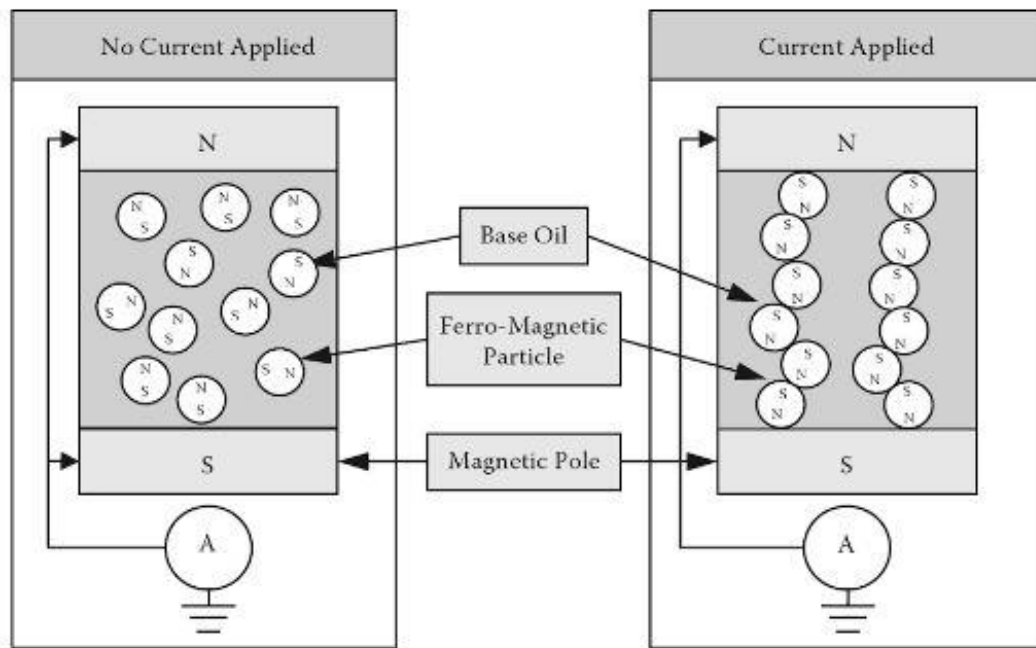


Figure 1.8 MR fluid in passive and active states (Choi & Han, 2013).

In the presence of a magnetic field, MR fluid is considered to be in its active state, when no external field is applied such a state of MR fluid is called passive. In the active state, MR fluid becomes semi-solid and behaves like a viscoelastic material before the shear stress reaches its yield value. After it passes the yield point, MR fluid exhibits viscoplastic nonlinear pseudoplastic behavior, i.e. viscosity is reduced with an increase of shear strain rate. The complete behavior and properties of MR fluid are quite complex and, thus, are described through a number of mathematical models to simplify the analysis of MR fluid technology based devices.

1.2.1. MR fluid models

Most popular and simple models to perform the analysis of MR fluid are typical non-Newtonian fluid models like Bingham model, Herschel-Bulkley model, Biviscous model, and Casson model.

Bingham model

The Bingham mathematical model, named after Eugene C. Bingham, describes a viscoplastic material as one that has a yield point (or a yield stress) and behaves like an elastic solid below this critical stress (Figure 1.9).

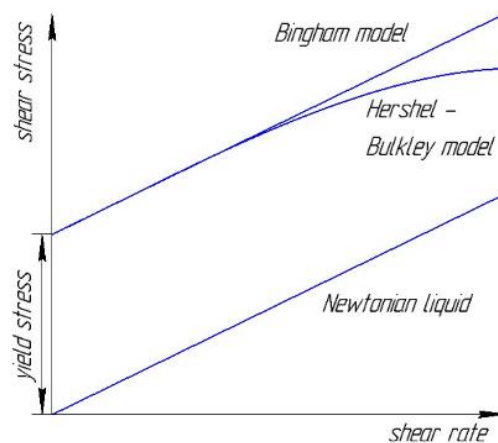


Figure 1.9 Comparison of Newtonian, Bingham, and Herschel-Bulkley models.

When the stress continues to increase and goes beyond the yield point, the material starts to flow like a liquid. With increasing magnetic fields, the yield stress of MR fluid also increases. The MR fluid yield stress is represented as a function of magnetic induction (Carlson & Jolly, 2000; An & Kwon, 2003):

$$\tau = \tau_y(B) \operatorname{sgn}(\dot{\gamma}) + \eta \dot{\gamma} \quad (2)$$

where τ is the shear stress, τ_y is the shear yield stress, $\dot{\gamma}$ is the shear strain rate, B is the magnetic field, and η is the post yield plastic viscosity.

Below the yield point, where material behaves like a solid, a general stress-strain relation for the shear is used:

$$\tau = G^* \gamma \quad (3)$$

The only difference is that the shear modulus is represented by a complex shear modulus G^* :

$$G^* = G' + iG'' \quad (4)$$

where G' and G'' are storage and loss moduli, respectively, and related to the energy stored and dissipated, respectively, per unit volume of the material during one loading cycle (Rajamohan, 2010).

Herschel-Bulkley model

The Herschel-Bulkley model describes viscoplastic material in a similar way as Bingham model (Figure 1.9). The only difference is that Herschel-Bulkley fluid experiences shear thickening or thinning, which is a nonlinear behavior (Yildirim, 2016). The mathematical model counts for this by introducing a flow behavior index into the Bingham model equation:

$$\tau = \tau_y(B) \operatorname{sgn}(\dot{\gamma}) + K(B) \dot{\gamma}^{n'} \quad (5)$$

where K is the consistency index, n' is the flow behavior index, which shows how much the fluid is susceptible to shear thinning or shear thickening.

Biviscous model

The biviscous model considers two yield stress values, static and dynamic yield stresses, and two viscosities, pre-yield and post-yield viscosities (Figure 1.10).

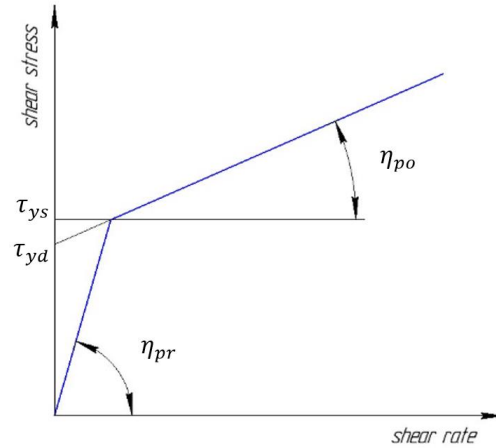


Figure 1.10 Biviscous model.

According to this model, in the regions where material experiences stress that is lower than static yield stress, the material behaves like a Newtonian fluid with a viscosity of pre-yield value. In the regions where the stress exceeds the static yield stress, the material behaves as a non-Newtonian fluid with much lower viscosity (post-yield viscosity) (Goncalves, 2005).

$$\tau = \begin{cases} \tau_{yd} + \eta_{po}\dot{\gamma}, & \tau > \tau_{ys} \\ \eta_{pr}\dot{\gamma}, & \tau \leq \tau_{ys} \end{cases} \quad (6)$$

where τ_{yd} is the dynamic yield stress, τ_{ys} is the static yield stress, η_{po} is the post-yield viscosity, and η_{pr} is the pre-yield viscosity.

Casson model

The Casson model describes a material as one that has a yield stress and behaves like a solid with a complex shear modulus G^* before reaching the yield point. After exceeding the yield stress, the Casson fluid starts to flow having an infinite viscosity at zero shear rate and gradually decreasing in a non-linear way to zero value at an infinite shear rate (Sidpara et al., 2009; Reddy, 2016; Pramanik, 2014):

$$\sqrt{\tau} = \sqrt{\tau_y} + \sqrt{\eta_{\infty}\dot{\gamma}} \text{ for } \tau > \tau_y \quad (7)$$

where η_{∞} is the suspension viscosity at infinite shear rate.

Abovementioned mathematical models are simplified and limited in complete explanation of the nature of MR fluid behavior. They were derived to satisfy the properties observed in experiments, and thus, in essence, represent phenomenological models (Ciocanel, 2006). Most of the components that constitute the equations are found empirically by curve fitting experimental results. In addition, ferromagnetic effect of solid particles in MR fluids is not considered. Consequently, a number of advanced models were developed to fully describe MR fluid behavior with a certain accuracy.

One of the advanced models is Kinetic Theory-based Model (Ahmadkhanlou et al., 2010), which is based on the first principles. This model uses kinetic equation to describe the rate of change of particles motion, counting for effects of carrier fluid flow, Brownian motion of the particles, intraparticle and external forces. Although the model shows very close results to the experimental values, it requires lots of parameters to be known and overcomplicates the analysis, and thus is used only if an exceptional accuracy of the results is required. Furthermore, a number of similar models that also use constitutive equations to derive MR fluid behavior were created (Ciocanel, 2006).

Another improvement in describing MR fluid is consideration of hysteresis in ferromagnetic particles. Two main models considering this effect are Preisach (Bertotti, 1998) and Hodgdon (Coleman & Hodgdon, 1986) models. For some applications to obtain an accurate solution, it is important to take a magnetic saturation into account, especially if particles are highly ferromagnetic and their volume fraction in the MR fluid is high.

Other advanced models are used for specific applications and designs. Some of them are obtained by combining known models (Guo et al., 2006) for more detailed, but still simple analysis of particular MR fluid device, e.g. MR damper. Some models are developed to improve the result for certain application, e.g. in case of high flow velocity and shear strain rate (Goncalves, 2005), where MR fluid “dwell time” should be considered. “Dwell time” is a term used to specify how long MR fluid is subjected to magnetic field, e.g. when passing through an orifice of MR fluid damper with locally subjected magnetic field in a piston. Counting for this factor is important to properly describe the dynamic characteristics of MR fluid.

1.2.2. MR fluid modes

In general, there are three main modes in which MR fluid based devices are operated (Figure 1.11).

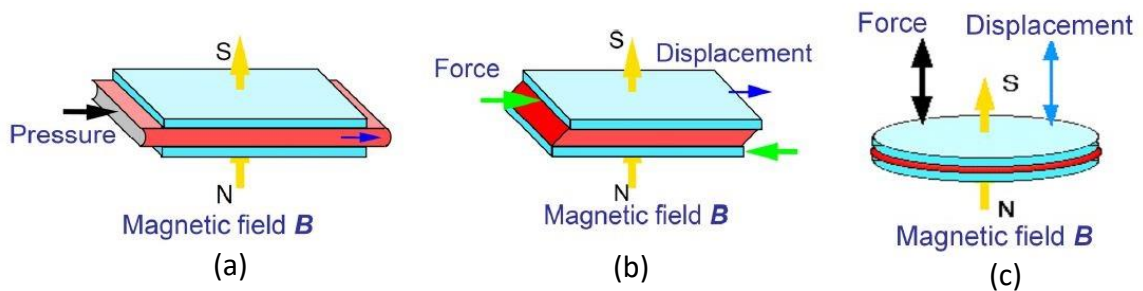


Figure 1.11 MR fluid (a) flow, (b) shear and (c) squeeze modes (Spaggiari, 2013).

In the flow mode, also called the valve mode, MR fluid flows due to pressure gradient between two parallel fixed walls. The shearing force is produced by viscous flow with a common velocity distribution, with zero velocity on the walls and maximum value in the middle of the gap. Such flow is typical for MR fluid valves, hydraulic dampers with orifices in the piston and bypass-type dampers etc. (Zhu et al., 2012).

In the shear operation mode, one of the walls is fixed while another is subjected to some displacement rate, or both parallel walls are moving in the opposite directions. This mode is typical to MR rotary shock absorbers, rotor brakes, and clutches (Spaggiari, 2013). Some configurations of MR damper use flow and shear combination mode. In this case MR fluid flows through the annular gap between a cylinder of a damper and its piston, as can be seen in Figure 1.12. Hence, the fluid flows due to displacement of inner wall (piston) while the second wall is stationary and the pressure gradient induced by the piston movement (Wang & Meng, 2001).

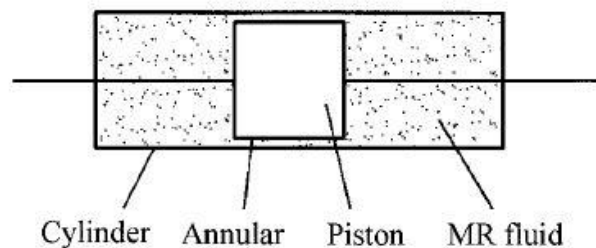


Figure 1.12 Flow and shear combination mode MR damper (Wang & Meng, 2001).

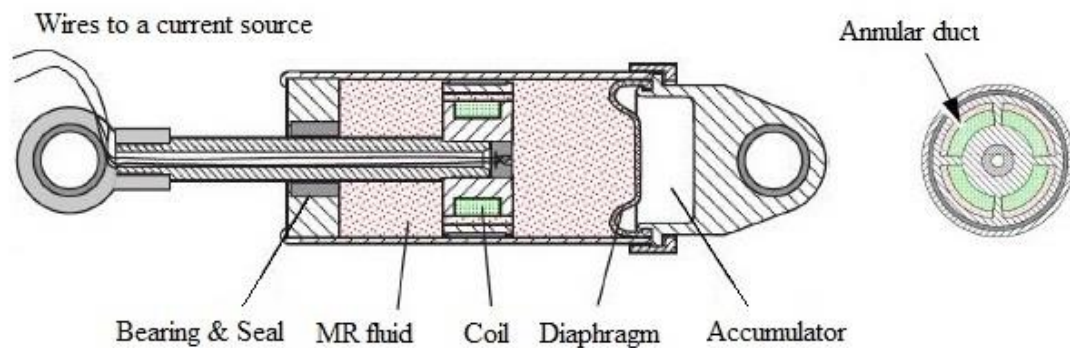
Finally, squeeze mode is the one where parallel walls are displaced relatively to each other in the transverse direction, i.e. along the magnetic field direction and solid particles chains. High pressure is produced between the plates and MR fluid flows from the center to the edges of the plates. Considering this, squeeze mode is able to produce high resistance force, but for small displacement. For that reason, it is mostly used for controlling low-amplitude vibrations (Zhu et al., 2012).

It can be mentioned, that in all the modes magnetic field is applied in the transverse direction to the walls. Being quite rough approximation for lots of MR devices designs, it often shows sufficiently accurate results. Hence, the assumption is considered reasonable for performing analysis of different applications.

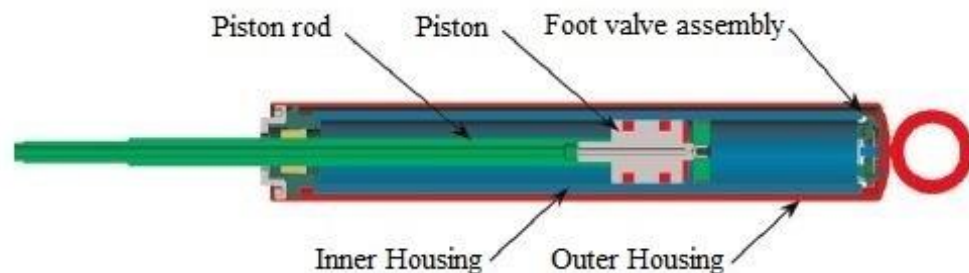
1.2.3. MR fluid devices

MR damper

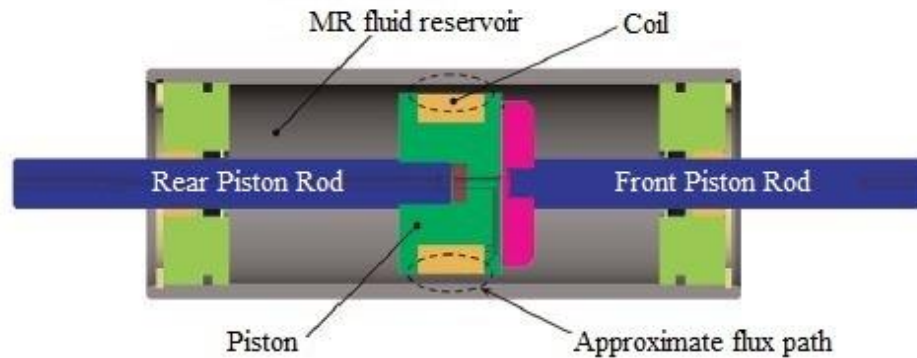
One of the most popular, studied and commercially successful MR fluid technology based devices is MR hydraulic damper. As it was mentioned in the previous section, there are different configurations of MR hydraulic dampers working in single and combined operational modes, shown in Figure 1.13 (a) and (c). Besides this, there is a number of MR damper configurations based on the number of chambers (Figure 1.13 (a) and (b)), number of piston rod (Figure 1.13 (a) and (c)), position (external or internal, perpendicular to or along the piston axis) and number of the coils (Figure 1.13 (d)), presence of bypass duct etc. (Zhu et al., 2012).



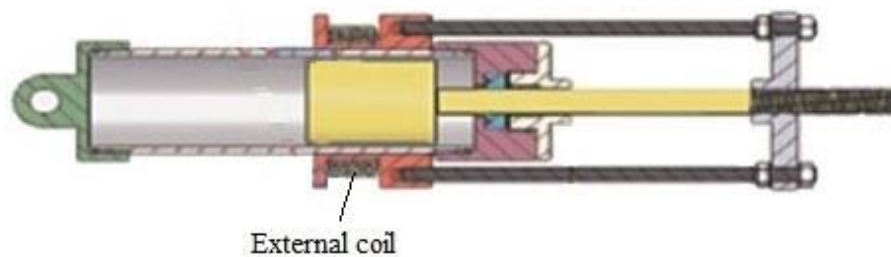
(a) Single chamber flow mode MR damper (Spaggiari, 2013)



(b) Double chamber MR damper (Poynor, 2001)



(c) Flow-shear mode MR damper (Poynor, 2001)



(d) MR damper with external coil (Zhu et al., 2012)

Figure 1.13 (a)-(d) MR dampers configurations.

Nevertheless, the principle of work of all the MR dampers is similar. Like in the case of common hydraulic oil damper, the piston movement causes certain pressure difference in the front and rear parts of a chamber. This pressure difference makes MR fluid to flow through some type of small orifice, depending on the configuration of a damper. The coil, installed in the damper, generates magnetic field that increases MR fluid viscosity within some volume around the orifice. By controlling the magnetic field strength, the certain amount of viscous drag is produced by MR fluid in the orifice, i.e. overall damping force can be also controlled and tuned in real-time to withstand external dynamically changing vibrations (Walid, 2002; Yang et al., 2002).

MR damper is already widely used in the automotive industry as an element of car primary and secondary suspension systems (Yao et al., 2002; Choi & Han, 2013). Several

companies manufacture and distribute the so-called smart suspensions. For instance, LORD Corporation sells separate MR damper units along with complete primary suspension systems for both civil and military vehicles, as well as seat suspensions (LORD website). Another company that sells primary car suspension systems is BWI Group (BWI website).

In Civil engineering large-scale MR fluid dampers are installed in bridges, high-rise buildings and other structures for wind and earthquake induced vibrations control (Xu et al., 2016).

In the aerospace industry, MR dampers are studied intensively for further implementation, particularly for helicopter application. These applications include crew seat suspension (Hiemenz, 2007; Gregory et al., 2008) for operation convenience as well as emergency action, rotor squeeze film damper (Forte et al., 2004) to reduce radial vibration of rotors, and finally for lead-lag blades vibration reduction (Ngatu et al., 2010; Kamath et al., 1999), which is so far the most promising application of MR damper in helicopters. Another common aerospace industry application of MR damper that is studied is landing gear vibration control (Choi & Wereley, 2003).

Besides these application, MR damper is used for smart prosthetics (Carlson et al., 2001) and even washing machines (Spelta et al., 2009).

MR mounts

MR mounts are used to support powertrains and power units and isolate them from the main frame of the structure. MR mounts work principle is very similar to the one of MR dampers, and usually they use some mix of operational modes of MR fluid. One of the configuration of MR mount studied is shown in Figure 1.14.

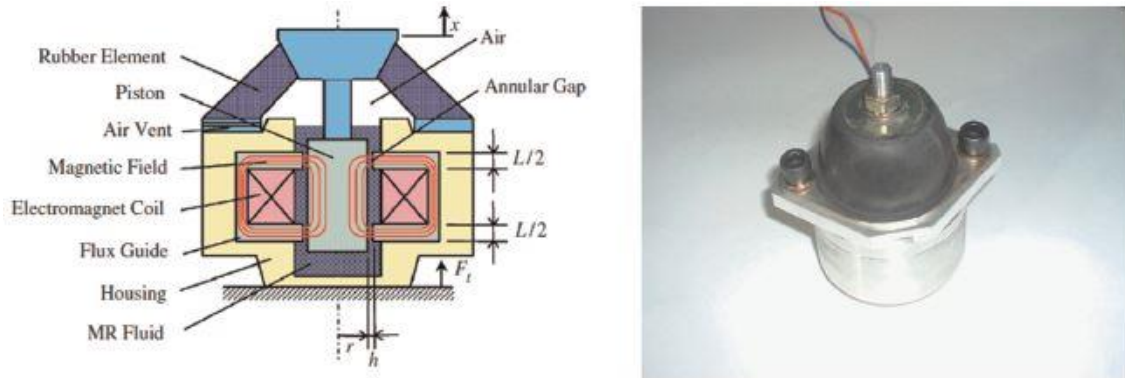


Figure 1.14 Configuration of and manufactured MR mixed-mode mount (Choi et al., 2008).

The successful performance of the device can again be proved by real industry application. The BWI Group, which was mentioned before, also sells MR mounts for car's powertrains, shown in Figure 1.15.

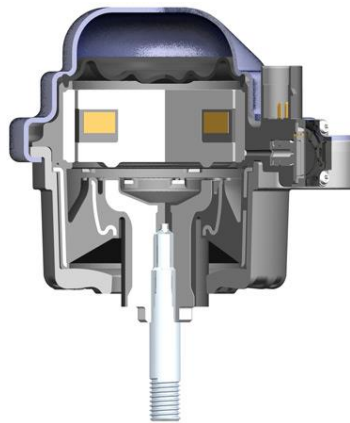


Figure 1.15 BWI Group MR mount for car powertrain (BWI website).

As it can be seen in Figure 1.15, the BWI Group MR mount uses flow operational mode of MR fluid, as orifice has an annular cross section and installed inside a piston-like part.

Brakes, Clutches and Steering Units

Applying MR fluid technology to rotary devices, a large number of advanced

properties was achieved. All the devices of this group are operated in shear MR fluid mode and have a quite similar configuration as can be seen in Figure 1.16.

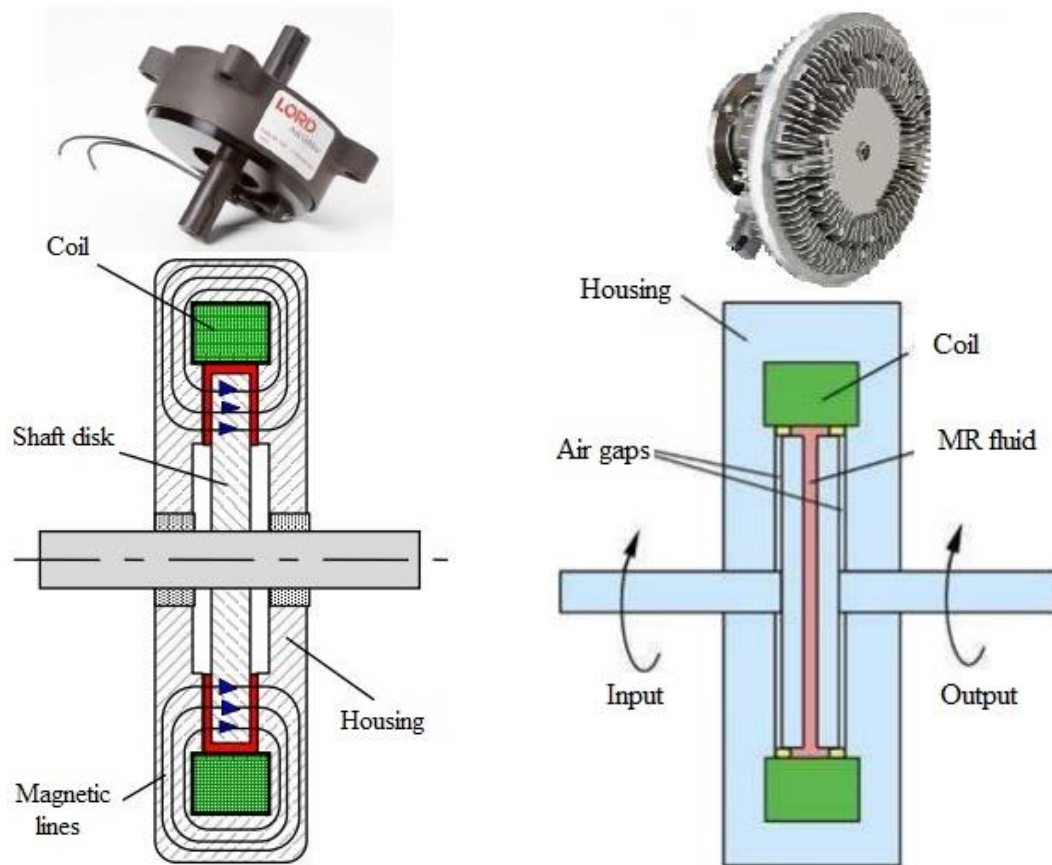


Figure 1.16 MR (a) brake and (b) clutch common configurations and commercial devices of LORD Corporation (Carlson et al., 2007; LORD, 2011).

The shaft is equipped with a disk, which plays a role of a moving plate in shear operational mode. The coil, installed outside the disk for maximum produced torque, generates magnetic field in such a way that magnetic lines pass MR fluid in the direction transverse to the disk. Hence, such a configuration is accurately described by shear operational mode.

Another device of this group is a Steering Unit, particularly Tactile Feedback Device (TFD). Using the same principle as abovementioned rotary devices, it produces a force to deliver a feedback to an operator. This is highly important in modern electronic

control systems, where controlling force is produced by some type of actuators (Vignesh, 2016). The importance of this device, and particularly success of MR fluid in this application, can be shown by LORD Corporation TFD steering unit (LORD website). The device entered the market in 1999, in 2006 around 50,000 of TFD were sold (Carlson et al., 2007), and nowadays more than 400,000 devices are in service (LORD, 2009). Although there is not enough data to be analyzed, one can mention that if some polynomial approximation is applied to the number of devices sold in corresponding years the curve would show exponentially growing interest to the device.

Besides the aforementioned, a variety of devices and different manufacturing processes based on MR fluid technology have been recently created and advanced, including MR fluid valves, polishing devices, etc. (Wang & Meng, 2001).

One interesting device utilizing MR fluid technology is a hollow helical spring filled with MR fluid, which was recently designed and investigated (Suresh et al., 2015). In the paper, analytical solution for the stiffness of such device and experimental results are presented. The spring was manufactured from silicon tube and later filled with MR fluid. Magnetic field was applied by copper wires coiled around the spring. The study showed that the MR fluid could control the stiffness of the silicone spring; however, the spring resistance force could be controlled in quite narrow range.

It was clear from the paper (Suresh et al., 2015) that applied magnetic field of 0.14 Tesla is fairly small for MR fluid to get its maximum yield stress. Moreover, only one spring design was considered, thus an additional improvement of MR fluid effect can be obtained by finding optimal design parameters. MR fluid filled spring has such advantages, comparing to other MR dampers, as simplicity in structure, high deflection ability (suitable

for high-amplitude vibration), potential lower weight (less MR fluid is used) and cost. In addition, in a relatively recent research on the controlling lead-lag vibration of the helicopter blades, a radial absorber based on Coriolis force was modeled and analyzed (Austruy, 2011). The results showed that such damper is able to suppress vibration by 35%, and hence, reduce the weight of blades by up to 5%. However, a spring or spring-like element with nonlinear stiffness is required to be used in such kind of radial damper. This effect can be achieved by utilizing MR fluid technology. Considering all these facts, an additional fundamental parametric analysis of the MR fluid filled spring is proposed in the present work.

Such an interest in MR fluid technology can be explained by its unique properties, such as high viscosity and shear stress when subjected to a magnetic field (in active state), rapid response (activation and deactivation time), low power consumption, and environmentally stable parameters. Furthermore, more advanced (Yang et al., 2015) and stable (Rodriguez-Lopez et al., 2015) MR fluids are developed (Ashtiani et al., 2014). In addition, an effect of yield stress increase was observed when MR fluid was subjected to some compression in the direction of magnetic lines, i.e. particle chains. The observed values of yield stress reached around 800 kPa (Tang et al., 2000) and 1100 kPa (Wang et al., 2008), which might be highly useful for some applications.

2. Objective and Approaches

Variable stiffness mechanical spring can be advantageous if used in modern active and semi-active damping systems. Although MR fluid is known to change its viscosity under magnetic fields, the effect of filled MR fluid on the stiffness of hollow spring has not been fully understood. Fundamental analytical study of a MR fluid filled spring in terms of stiffness change is the main objective of this paper.

The changes in stiffness of the MR fluid spring system are calculated using advanced spring mechanics, fundamentals of fluid mechanics, and MR fluid rheology. Numerical solution is used to simplify the complex transient processes and to prove some assumptions made in the analytical solutions. To investigate the performance of the MR fluid filled spring, its stiffness changes are investigated with design parameters of the hollow spring, such as spring index, pitch angle, cross-sectional void ratio, and spring.

3. Analytical Approach

3.1. Spring mechanics

In order to calculate the stiffness of the MR fluid filled spring, the stiffness of a hollow spring and its mechanical equations are first considered. Main geometrical parameters of the helical spring with annular cross section are shown in Figure 3.1.

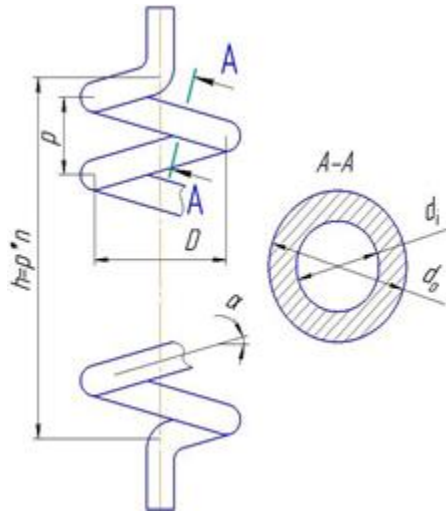


Figure 3.1 Geometry of a helical hollow spring with annular cross section.

In the figure, D is the spring mean diameter, p is the pitch distance, α is the pitch angle, h is the length of the spring, n is the number of coils, d_i and d_o are inner and outer radii of the annular cross section, respectively. Two more main spring parameters are a spring index and a void ratio of the annular cross section. Spring index, $i = D/d_o$, is the ratio of a spring mean diameter to an outer radius of the circular or annular cross section. Void ratio, $\xi = d_i/d_o$, is the ratio of inner to outer radii of the annular cross section.

In general, when a helical spring is subjected to a tensile or compressive load, its coil is loaded by four loads, i.e. torsion, bending, shearing and axial forces (Ciupitu & Simionescu, 2014). These loads represent stiffness components by which a spring resists its deformation under the total load applied. The values of these components, or the ratios

between them, depend on the geometry of a spring and its cross section. A number of approaches to calculate the stiffness of the helical spring were developed. For manufacturing purposes, large index and small helix angle springs are often designed using the elementary (or classical) spring theory (Wahl, 1944). This theory neglects the pitch angle of a spring, which causes bending and tension, and a curvature of its wire. Moreover, the theory often neglects the shear component as it is smaller than torque for a large index spring. As a result, a spring is considered as a straight shaft loaded by a torque only and the stiffness of a spring can be represented as (Wahl, 1944):

$$k = \frac{GJ_p}{2n\pi R^3} \quad (8)$$

where G is a shear modulus of the spring material; J_p is a polar moment of inertia of the spring cross section; n is the number of spring coils; and R is the mean radius of the spring.

Despite the simplicity of the elementary theory, it provides quite accurate results for a spring with large index and small pitch angle. However, there are many other cases that different loading and geometric relations are demanded, such as a highly loaded spring with small index or a highly deflection spring with large pitch angle. Therefore, a fundamental study of the spring stiffness with corresponding mechanical properties is needed.

To improve the accuracy of the calculations for a spring with low and moderate index values, curvature of the spring wire and the effect of shearing force must be considered. Here, the distribution of stress, induced by torque, becomes non-linear and an effect of direct shear from the force applied can be considered by a correction factor. The two most known solutions of such type of approach are Wahl's (Wahl, 1944) and Timoshenko's (Gere & Timoshenko, 1991) equations and their correction factors. These

approaches give an error no more than 2% for stress calculations for closed-coiled springs with an index equal to 3, and are even more accurate for the stiffness calculations (Gere & Timoshenko, 1991).

When a spring has a moderate or large pitch angle, such as an open-coiled spring, bending and sometimes tensile force should be taken into account as well. However, the tensile force portion is often neglected as it constitutes less than 1% of the overall stiffness of a spring with high pitch angle and low index, when the tensile portion gets its largest value.

To simplify calculations, a number of equations were developed for particular spring designs. For instance, the following equation considers torque and bending such that it is accurate for springs with moderate or high index when shearing component becomes small (Love, 1927):

$$F = \frac{\gamma C}{R} \left(\frac{SC}{R} - \frac{S_0 C_0}{R_0} \right) - \frac{\beta S}{R} \left(\frac{C^2}{R} - \frac{C_0^2}{R_0} \right) \quad (9)$$

where γ and β are the torsional and flexural rigidities of the spring coil, respectively. $S(C)$ and $S_0(C_0)$ are sin (cos) functions of the pitch angle after and before deformation, and R_0 and R are the mean radii of the spring before and after deformation, respectively.

All those equations, besides the elementary theory, are based on or partially use principles of the theory of elasticity. There are also some solutions obtained using a finite element method to increase the accuracy of calculations and to be able to study boundary effects (Fakhreddine et al., 2005).

Another relatively simple approach of calculating the stiffness, by considering all four loads acting in the spring, is an energy method, particularly Castigliano's second theorem. A solution using this method was obtained for different geometries of the spring

and its cross section. The results of the solution were compared with the results of other methods and showed sufficient accuracy for various spring dimensions. According to this approach, the deflection of each load component can be shown (Yildirim, 2016):

$$\delta_{T_b} = \frac{2Pn\pi R \cos \alpha}{C_b} \quad (10)$$

$$\delta_{T_t} = \frac{2Pn\pi R \sin \alpha \tan \alpha}{C_t} \quad (11)$$

$$\delta_{M_b} = \frac{2Pn\pi R^3 \sin \alpha \tan \alpha}{D_b} \quad (12)$$

$$\delta_{M_t} = \frac{2Pn\pi R^3 \cos \alpha}{D_t} \quad (13)$$

where δ_{T_b} , δ_{T_t} , δ_{M_b} , δ_{M_t} are deflection components of shearing force, axial force, bending, and torsional moments, respectively, P is the total load applied to the spring, C_b , C_t , D_b , D_t are shearing, axial, bending and torsional rigidities of the spring coil cross section, respectively.

Using these equations, the stiffness components of different spring designs can be compared. With some calculations, it is found that the major loads affecting the spring stiffness are the spring index and the pitch angle. The ratios of all four stiffness components with different spring indices and pitch angles are shown in Figure 3.2.

The results show that torsion component is the most significant factor that accounts for more than 90% of the overall stiffness for the majority of spring designs used in industries. The torsion component becomes larger with increased spring index or decreased pitch angle. Bending component gets bigger as each of these two spring geometric parameters increases. Shear component gets significantly smaller with the increase of spring index, while it has almost no effect with a pitch angle, showing slightly decreasing

the stiffness with increased pitch angle. As expected, a tension component of stiffness is comparably low, not exceeding 0.5% for a spring with low index and high pitch angle.

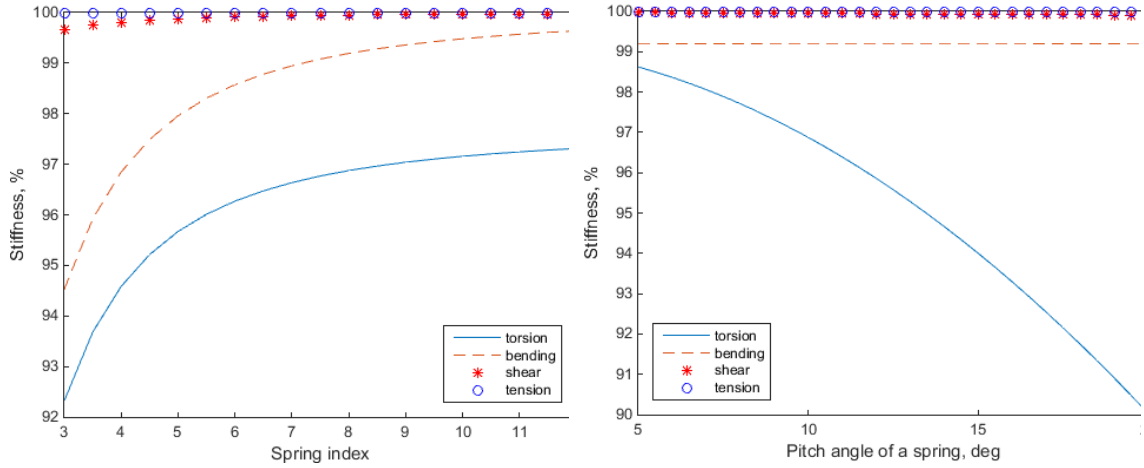


Figure 3.2 Stiffness components of the spring with change of a spring (a) index ($\alpha = 10^\circ, d = 10$ mm), (b) pitch angle ($i = 8$ – spring index, $d = 10$ mm).

In our case, the coil of the spring is represented by a tube, which changes the ratio of the above mentioned components as well. Bending and torsional stresses have smaller values in the center of the cross section, while stresses from tension and shearing force are distributed uniformly. Thus, lack of material in the center of the cross section influences shear and tension components more than bending and torsion components. As tension component is assumed to be small, the change of it is also neglected. As a result, only a shear correction factor, which is a function of the material Poisson's ratio and the cross section geometry, is used. Hence, the expression for calculating the stiffness of the spring with annular cross section is (Yildirim, 2016):

$$k = \frac{G(1 + \nu)(d_0^4 - d_i^4)}{4nR \cos \alpha \left(16R^2(\nu + \sec^2 \alpha) + (d_0^2 + d_i^2)(2(1 + \nu)k_n + \tan^2 \alpha) \right)} \quad (14)$$

where ν is the Poisson's ratio of the material and k_n is the shear correction factor:

$$k_n = \frac{(7 + 6\nu)(1 + \xi^2)^2 + (20 + 12\nu)\xi^2}{6(1 + \nu)(1 + \xi^2)^2} \quad (15)$$

3.2. Analytical approach on MR fluid

According to the Bingham model, MR fluid can exist in both elastic solid and viscoplastic states. As a result, the total change in stiffness due to adding MR fluid to the hollow spring is divided into pre-yield and post-yield portions of MR fluid stiffness. Thus, before yielding, MR fluid can be considered as a spring made of some elastic material with shear modulus being equal to the MR fluid complex shear modulus. The stiffness of such spring can be calculated using Wahl's corrected formula for a circular cross section (Wahl, 1944):

$$k_{MRF}^{pre-yield} = \frac{G^* J_p^*}{2n\pi R^3} \left(\frac{i_{MRF}^2}{i_{MRF}^2 + 0.5} \right) \quad (16)$$

where G^* is the complex shear modulus of the MR fluid, $J_p^* = \pi r^{*4}/2$ is the polar moment of inertia of the MR fluid solid core, and $i_{MRF} = R/r^*$ is the index of the MR fluid spring, where r^* is the radius of the MR fluid solid core.

Different expressions for the complex shear modulus G^* were found in previous works. Equations (17) – (18) were found experimentally using the ASTM E756-98 Standard (Naji et al., 2016):

$$G'(B, f) = (9.63 * 10^4 - 1.51 * 10^2 * B + 9.0 * 10^{-2} * B^2) + (6.39 * 10^3 - 2.54 * B - 8.47 * 10^{-4} * B^2) f [Pa] \quad (17)$$

$$G''(B, f) = (2.70 * 10^4 + 6.70 * B + 4.5 * 10^{-2} * B^2) + (3.80 * 10^2 + 7.0 * 10^{-1} * B - 2.20 * 10^{-4} * B^2) f [Pa] \quad (18)$$

$$G^*(B, f) = G'(B, f) + jG''(B, f) \quad (19)$$

where B is the magnetic induction ($0 \leq B \leq 2000$ Gauss) and f is the frequency ($0 \leq f \leq 400$ Hz).

Likewise, Equations (20) – (21) were obtained by fitting the experiment results data, for instance (Rajamohan et al., 2010):

$$G'(B[Ts]) = -3.3691 * B^2 + 4997.5 * B + 0.873 * 10^6 [Pa] \quad (20)$$

$$G''(B[Ts]) = -0.9 * B^2 + 0.8124 * 10^3 * B + 0.1855 * 10^6 [Pa] \quad (21)$$

As well as Equations (22) – (23) (Sun et al., 2003):

$$G'(B[Gauss]) = 3.11 * 10^{-7} * B^2 + 3.56 * 10^{-4} * B + 5.78 * 10^{-1} [MPa] \quad (22)$$

$$G''(B[Gauss]) = 3.47 * 10^{-9} * B^2 + 3.85 * 10^{-6} * B + 6.31 * 10^{-3} [MPa] \quad (23)$$

The equations show that the maximum shear modulus of MR fluid MRF-132DG, obtained by applying the magnetic field in a reasonable range, usually do not exceed the value of 3-4 MPa. After the solid component of MR fluid stiffness is calculated, MR fluid viscous contribution is to be determined.

MR fluid goes from solid to a viscous state when the stress exceeds the yield point, which for MRF-132DG can be found according to one of the equations shown (Thakkar et al., 2013; Suresh et al., 2015):

$$\tau_y(B) = 52.962 * B^4 - 176.51 * B^3 + 158.79 * B^2 + 13.708 * B + 0.1442 \quad (24)$$

$$\begin{aligned} \tau_y(B) = 39.7215 * B^4 - 132.3825 * B^3 + 119.0925 * B^2 + 10.281 * B \\ + 0.10815 \end{aligned} \quad (25)$$

According to the elementary theory, a spring is considered as a straight shaft and shear stress distribution in the circular cross section is assumed to be linear, changing from zero at the center to the maximum value at the edge. Therefore, the stress reaches the yield point of the MR fluid at the outer regions first. While the stress keeps growing, more MR fluid goes from solid to fluid state. To calculate the viscous, or post-yield, portion of MR fluid stiffness, this solid-fluid boundary location should be found for a given load, magnetic

field, material, and geometry of the spring. Shear strain for the shaft is calculated using the following equation (Pumnia et al., 2002):

$$\gamma = \frac{2r\varphi}{\pi R} \quad (26)$$

where r is the radius of the cross section at which shear strain is calculated, and φ is the angle of twist, which is calculated for the spring according to the elementary theory (assuming only torque):

$$\varphi = \frac{\delta}{4nR} \quad (27)$$

Substituting Equation (27) into (26) and introducing a new variable, a relative deflection of a spring, $\bar{\delta} = \delta/h_0$, where $h_0 = pn$ is the height of a spring before deformation and $p = 2\pi R \tan \alpha$ is a pitch of a spring, we obtain:

$$\gamma = \frac{r}{R} \bar{\delta} \tan \alpha \quad (28)$$

The radius of the solid-fluid boundary, r^* , can be found from the value of shear stain, γ_y , that corresponds to the shear yield stress, τ_y :

$$\gamma_y = \frac{\tau_y(B)}{G^*(B)} = \frac{r^*}{R} \bar{\delta} \tan \alpha \Rightarrow r^* = \frac{\tau_y(B)}{G^*(B)} \frac{R}{\bar{\delta} \tan \alpha} \quad (29)$$

The flow of MR fluid in viscous state in the cross section (between hollow spring and solid MR fluid) can be represented as a transient flow between two concentric rotating cylinders (Figure 3.3). In the figure, $r_i = d_i/2$ is the inner radius of the hollow spring annular cross section, r^* is the radius of the solid-fluid boundary, V is the velocity distribution (shown linear for steady flow) and y is the variable used in Equation (31) – (33).

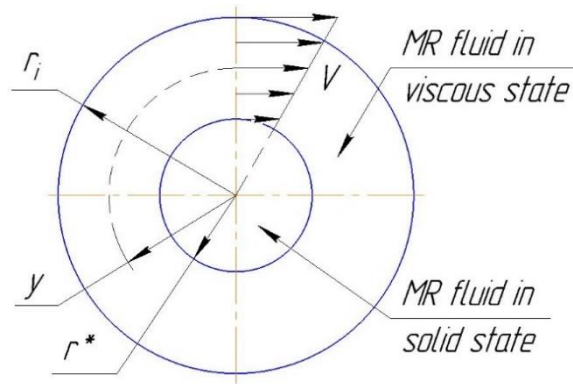


Figure 3.3 Linear flow between two concentric rotating cylinders.

Due to high viscosity of MR fluid and low shear strain rates in a helical spring, the transient flow of MR fluid is assumed to become steady-state very quickly. To proof this assumption, the simulation is performed for MR fluid flow induced by rotating inner (MR fluid core) and outer (inner wall of the spring cross section) cylinders. From the simulation, it can be seen that for low and moderate deflection rates of the spring, the flow distribution between these two cylinders changes from nonlinear (transient) to linear (steady) in a negligible amount of time (Figure 3.4). Considering this, the flow can be assumed to be steady-state initially.

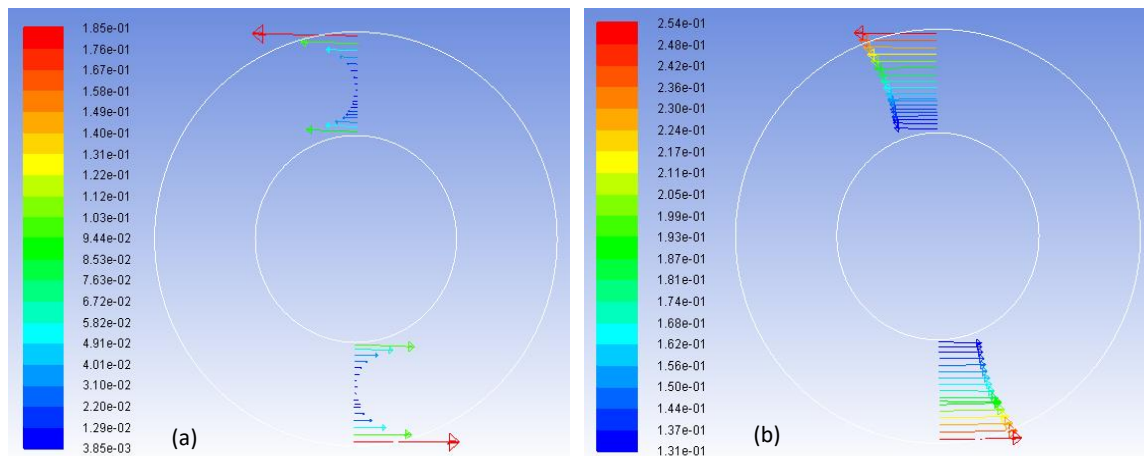


Figure 3.4 Velocity profile (mm/s) for transient flow in the spring cross section at the moment of: (a) 0.2% spring elongation or $t=0.001$ s; (b) 4% spring elongation or $t = 0.02$ s ($f = 1$ Hz, $t = 1/2f = 0.5$ s, $\delta = 10.75$ mm, deflection rate = $\delta/t = 21.5$ mm/s, $r^* = 0.25d_i$, $d_i = 7$ mm, $R = 17.5$ mm, $n = 4$).

The linear velocity distribution of the steady-state flow between two concentric rotating cylinders can be verified by an exact solution of Navier-Stokes equation (IIT Kanpur, 2009). Hence, the steady state equation of fluid mechanics can be used in this case:

$$\tau = \frac{\mu V}{r_i} \quad (30)$$

where μ is a viscosity of the fluid, V is the velocity at given y , and r_i is the inner radius of the cross section (Figure 3.4).

From Figure 3.3:

$$V = \frac{y}{r_i} V_{max} \quad (31)$$

where y goes from r^* to r_i (Figure 3.3).

Then, the stress in MR fluid can be shown as:

$$\tau = \mu V_{max} \frac{y}{r_i^2} + \tau_y \quad (32)$$

The resistance moment of the post-yield MR fluid is:

$$M = \int \tau y dA = \frac{\mu V_{max}}{r_i^2} \int y^2 dA + \tau_y \int y dA \quad (33)$$

where $\int y^2 dA$ is a polar moment of inertia J_p .

Hence, the post-yield force is:

$$F_{MRF}^{post-yield} = \frac{\mu V_{max}}{r_i^2} \frac{\pi(r_i^4 - r^{*4})}{2R} + \tau_y \frac{2\pi(r_i^3 - r^{*3})}{3R} \quad (34)$$

The maximum speed of the flow is equal to the speed of the moving wall, assuming no-slip condition. Thus, it can be calculated for the given loading frequency:

$$V_{max} = \omega r_i = \frac{\varphi}{1/2f} r_i = 2f\varphi r_i = \frac{f\delta}{2nR} r_i \quad (35)$$

Substitute this into the Equation (34):

$$F_{MRF}^{post-yield} = \frac{\mu}{r_i} \frac{\pi \delta f}{4nR^2} (r_i^4 - r^{*4}) + \tau_y \frac{2\pi}{3R} (r_i^3 - r^{*3}) \quad (36)$$

Therefore, the overall stiffness portion of the MR fluid is obtained as:

$$k_{MRF} = k_{MRF}^{pre-yield} + k_{MRF}^{post-yield} \\ = \frac{G^* r^{*4}}{4nR^3} \left(\frac{i_{MRF}^2}{i_{MRF}^2 + 0.5} \right) + \frac{\mu}{r_i} \frac{\pi f}{4nR^2} (r_i^4 - r^{*4}) + \tau_y \frac{2\pi}{3R\delta} (r_i^3 - r^{*3}) \quad (37)$$

For a given spring design, MR fluid stiffness component can be evaluated for different spring loading cases, i.e. different spring deflections and frequencies of the load applied. The corresponding stiffness variation can be seen in Figure 3.5. For convenience, relative spring deflection $\bar{\delta} = \delta/h_0$ is used instead of absolute value of it. The figure shows that for some initial range of the relative deflection the stiffness is constant, as all the MR fluid stays in the solid state. After some value of the relative deflection is reached, MR fluid stiffness starts to reduce significantly. This is the point, when the stress on the edge of MR fluid reaches the yield stress and MR fluid starts to transmit to liquid (post-yield) state. As relative deflection increases, the radius of the fluid-solid boundary r^* decreases, which greatly reduces the pre-yield MR fluid stiffness. Although, the post-yield MR fluid region is increased, its stiffness is not high enough to compensate the overall stiffness drop. It is observed, that the change in viscous component of the post-yield MR fluid stiffness is not noticeable with variation of the frequency of the load applied. To be able to evaluate the viscous portion for a wider range of spring designs, its ratio to the overall MR fluid stiffness is calculated for the different spring indices and pitch angle values with a constant magnetic field (Figure 3.6).

For consistency, the spring geometry in Figure 3.5 and Figure 3.6 is taken the same as in the previous study of the MR fluid spring (Suresh et al., 2015).

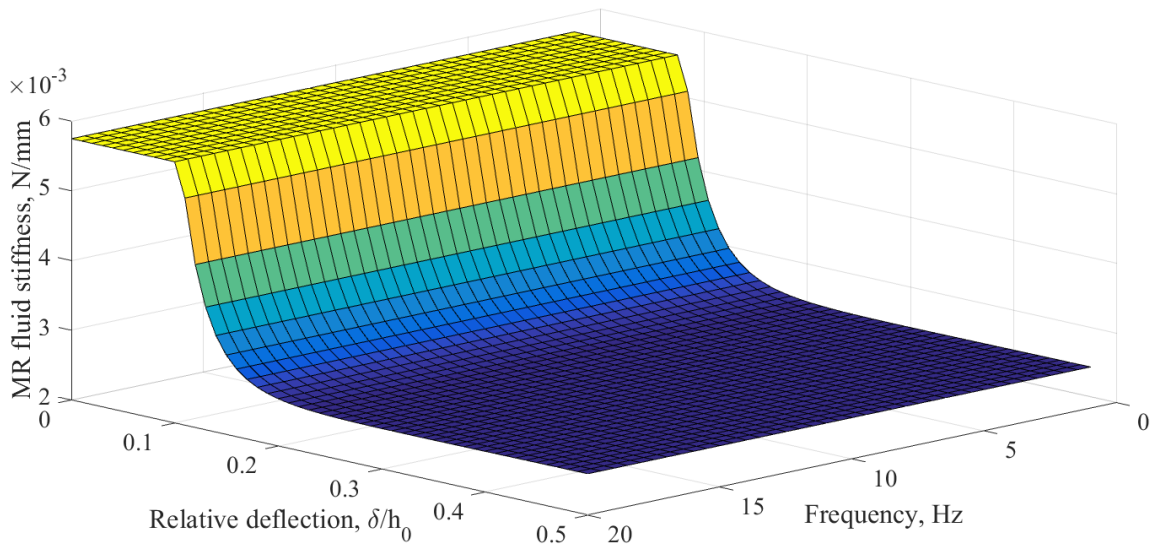


Figure 3.5 MR fluid stiffness portion $k_{MR\ fluid}$ with change of relative deflection $\bar{\delta}$ and loading frequency f ($d_i = 7$ mm, $i = 4.375$, $\xi = 0.875$, $\alpha = 5.3^\circ$, $n = 4$, $B \approx 0.14$ Ts, $G^* = 3.35$ MPa, $\tau_y = 6.6$ kPa).

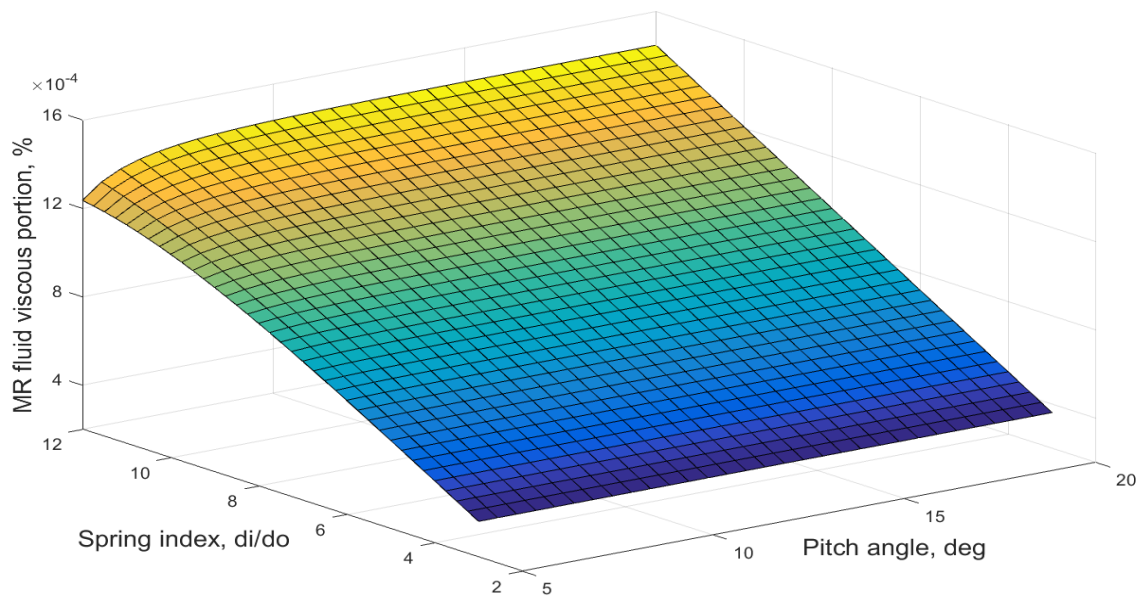


Figure 3.6 Viscous portion of MR fluid stiffness for different spring designs ($f = 20$ Hz, $\bar{\delta} = 0.5$, $d_i = 7$ mm, $\xi = 0.875$, $n = 4$, $B \approx 0.14$ Ts, $G^* = 3.35$ MPa, $\tau_y = 6.6$ kPa).

It is appeared that the viscous portion grows up to 0.0014% for the spring with the index of 12, which is the highest commonly used spring. Variation of pitch angle does not

show any perceptible change in the viscous component. This is due to the fact that the equation used to calculate the solid portion of MR fluid stiffness considers only torque and shear. Hence, the above results for different values of the pitch angle are not completely accurate, as Wahl's corrected formula (Equation 16) shows excess stiffness values for high pitch angles. However, the error in Wahl's corrected formula is shown to be less than 5% for a spring with the pitch angle of 20 degrees and 15% for the pitch angle of 40 degrees (Yildirim, 2016). Thus, this error is not significant in our case and the viscous portion of MR fluid stiffness can be neglected.

The above conclusion is made with the assumption that the flow between two concentric rotating cylinders is linear, when for high loading frequencies of the spring, the flow cannot be assumed steady or linear. For transient non-linear flow between two concentric rotating cylinders, the speed gradient is much higher at the outside boundary comparing to steady state flow, but rapidly falls at some relatively small distance from the boundary. Thus, higher shear stress is produced close to the boundary only. This increases the viscous portion of MR fluid stiffness in some magnitude but does not make it sufficient enough to be considered in the calculations of the overall MR fluid stiffness.

Finally, the equation to calculate the overall stiffness of the spring filled with MR fluid can be obtained:

$$k = \frac{G(1 + \nu)(d_0^4 - d_i^4)}{4nR\cos\alpha \left(16R^2(\nu + \sec^2\alpha) + (d_0^2 + d_i^2)(2(1 + \nu)k_n + \tan^2\alpha) \right)} + \frac{G^*(B)r^{*4}}{4nR^3} \left(\frac{i_{MRF}^2}{i_{MRF}^2 + 0.5} \right) + \tau_y \frac{2\pi}{3R\delta} (r_i^3 - r^{*3}) \quad (38)$$

4. Results of Analytical Approach

In the previous study (Suresh et al., 2015), the force to spring elongation relation (or stiffness) was obtained analytically and experimentally for a MR fluid spring made of silicon, filled with MRF-132DG. In their analytical solution, the elementary theory was used to calculate the stiffness of the hollow spring and the MR fluid stiffness component was calculated using the approach developed by the authors. In the experiment, the silicon spring filled with MR fluid was tested by attaching the ends to the force sensor and linearly varying a displacement ladder. An electromagnetic field was applied by means of copper wire wound around the spring coil. According to their results, the analytical solution estimated the resistant force of the spring of 0.171 N for 35 mm of the spring deflection, while the experiment measured the force of 0.212 N for the same spring deflection. The difference between these values is 21.4%.

Using the equation for the stiffness of MR fluid filled spring derived in the present work (Equation 38), the analytical solution shows the resistant force of the spring of 0.201 N for 35 mm of the spring deflection (Figure 4.1).

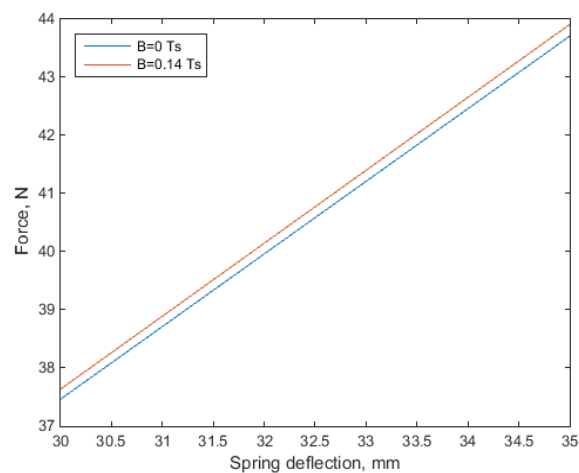


Figure 4.1 Force – deflection relation of the MR fluid filled spring obtained in the present study.

The difference between the analytical solution and experiment result from the previous study is reduced to 5.3%. The present calculations are performed with the same to the previous study inputs, i.e. spring geometry, MRF-132DG properties (LORD, 2011; Suresh et al., 2015), mathematical model (Bingham model), and magnetic field (calculated using Biot-Savart law, where magnetic permeability of MRF-132DG $\mu_r = 7$ is used (Simon et al., 2001)).

Finally, as the analytical solution is validated from the experimental study with a small margin of error, the MR fluid filled spring stiffness can be further studied for different spring designs with a constant magnetic field ($B = 0.14$ Ts). Main parameters controlling the design of the MR fluid filled spring are spring index, pitch angle of the spring, void ratio of the annular cross section, and the material used for the hollow spring. Stiffness of the hollow spring and MR fluid filled spring, as well as percentage contribution of MR fluid stiffness to MR fluid filled spring stiffness, are shown as functions of abovementioned design parameters in Figure 4.2.

Figure 4.2 (a) and (b) show that the variation of spring parameters, such as spring index (3 to 12) and pitch angle (5° to 20°), contributes very little in the overall MR fluid filled spring (MR fluid contribution 0.8% and 0.2%, respectively, for the hollow spring geometry and material shear modulus given). Accordingly, these parameters are not useful in terms of controlling the maximum contribution of MR fluid to the overall stiffness. It should be mentioned that Figure 4.2 (b) is not completely accurate for large values of the pitch angle because Wahl's corrected formula (Equation 16), which accounts for variation of spring the index only, is used in the calculation of the solid contribution of MR fluid stiffness.

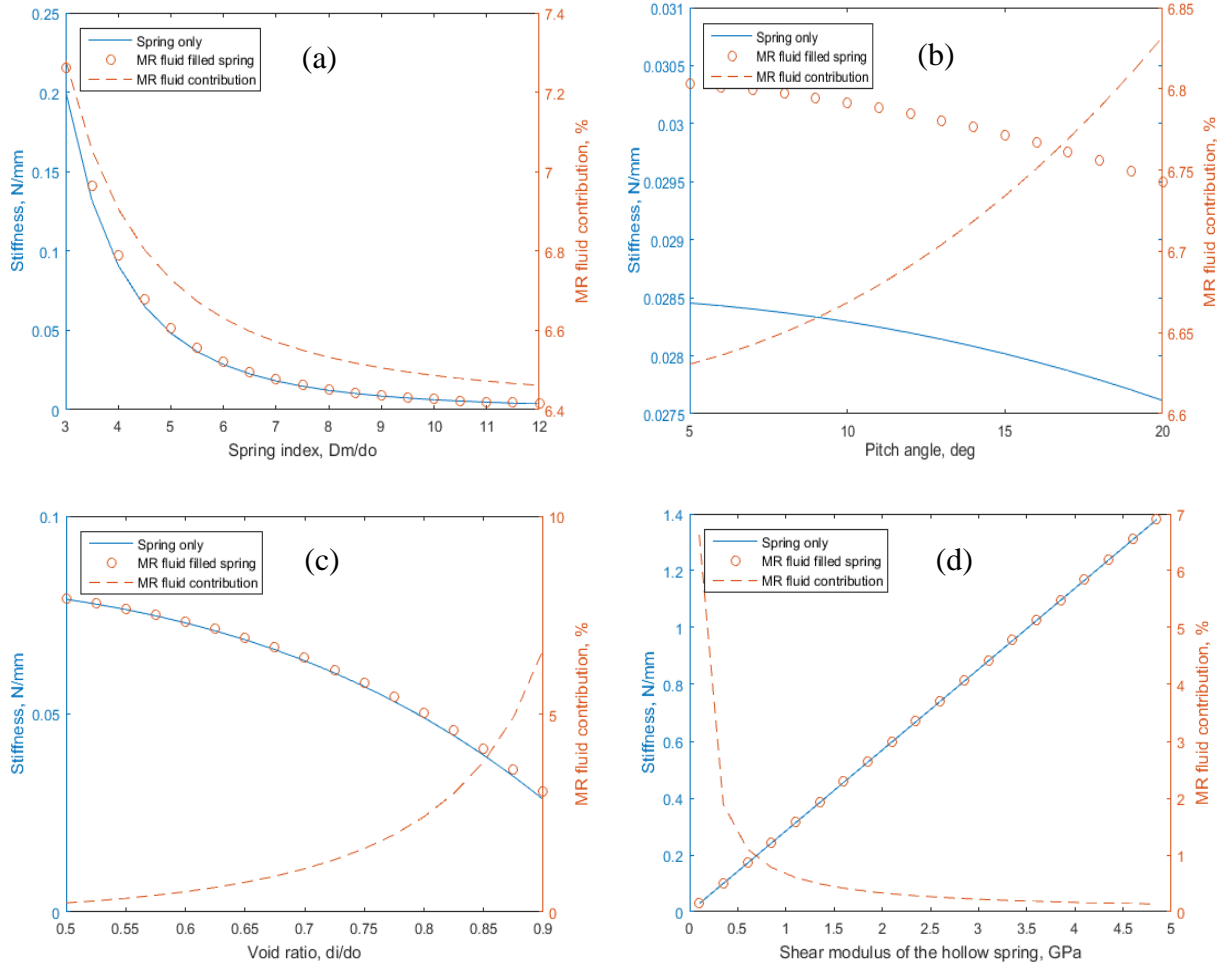


Figure 4.2 Stiffness of the hollow spring and MR fluid for different: (a) spring index ($G = 0.1$ GPa, $\alpha = 5^\circ$, $\xi = 0.9$), (b) pitch angle ($G = 0.1$ GPa, $\xi = 0.9$, $i = 6$), (c) void ratio ($G = 0.1$ GPa, $\alpha = 5^\circ$, $i = 6$), (d) shear modulus of the hollow spring material ($i = 6$, $\alpha = 5^\circ$, $\xi = 0.9$).

From Figure 4.2 (c), it can be seen that the void ratio of the annular cross section is an important factor that controls MR fluid stiffness contribution. To enhance the effect of MR fluid the void ratio of the annular cross section of the helical spring must be maximized. Finally, Figure 4.2 (d) shows that materials with low shear modulus must be used for a hollow spring (less than 1 GPa) to obtain some noticeable MR fluid stiffness contributions. Hence, two major design parameters that determine the final performance of the MR fluid filled spring are the cross section void ratio and the shear modulus of the

hollow spring.

To increase the controllable portion of MR fluid filled spring stiffness, the void ratio of the annular cross section must be as large as possible. However, an increase of the void ratio leads to a decrease of the wall thickness and can cause local buckling of the spring. To prevent local instability of the spring, the largest safe value of the void ratio must be used. The solution for the void ratio of the annular cross section, providing spring local stability (Spinella & Dragoni, 2010), shows the value of about 0.875 for springs made of stainless steel (for a reasonable value of safety factor). For most of materials, this value fluctuates between 0.8 and 0.9. It should be noticed that this void ratio value considers only the local buckling load based on the operational load as well as some factor of safety values to account for dynamic loading. Nevertheless, the manufacturing of a spring with high void ratio is a challenging process because thin walls tend to deform during the spring manufacturing process.

Most of the helical springs are manufactured from different steel alloys due to their processing and fatigue advantages. Some springs are manufactured of titanium alloys to reduce their weight and improve corrosion resistance (MW Industries, 2016). Titanium springs have lower shear modulus than the one of steel alloys, about 42 GPa and 80 GPa, respectively. However, for specific applications, springs can be made of different polymers, e.g. silicon, the low shear moduli of which are suitable for MR fluid filled application as it exhibits noticeable controllable portion of the stiffness.

To show the performance of MR fluid spring with close-to-optimum design, the derived equation for the overall stiffness (Equation 38) is used for a range of operational magnetic field values.

While most of values are well known or can be calculated, the complex shear modulus of MR fluid as a function of magnetic field is usually obtained empirically. In addition, three sets of equation for storage and loss shear moduli mentioned above are accurate for some range of magnetic field, but show excessive values of moduli for zero magnetic field. Another research on the MR fluid is considered (Laun et al., 2010) in which the moduli are measured with a rheometer for multiple points from zero magnetic field to 0.78 Ts, and are shown in Table 4.1.

Table 4.1 Magnetic field (flux density) dependent values of yield stress and shear moduli (Laun et al, 2010).

Flux density B (T)	Yield stress τ_Y (kPa)	Loss modulus G'' (kPa)	Storage modulus G' (kPa)
0	0.041	0.82	2.1
0.05	0.57	69	160
0.19	6.6	220	2200
0.39	20	82	3000
0.78	54	52	3500

The given values of shear moduli are interpolated with second order Lagrange polynomial approximation:

$$G'(B[\text{Gauss}]) = -1.201 * 10^{-4} * B^2 + 1.386 * B + 2.1 [\text{kPa}] \quad (40)$$

$$G''(B[\text{Gauss}]) = -1.85 * 10^{-5} * B^2 + 0.151 * B + 0.85 [\text{kPa}] \quad (41)$$

These expressions show a gradual nonlinear growth of the storage modulus from zero magnetic field to about 0.6 Ts, where it almost reaches 4 MPa. The value of the magnetic field for which the modulus gets its maximum value is also reasonable as it coincides with the saturation point of most MR fluids, after which the yield stress does not increase (An & Kwon, 2003). Applying these values of shear moduli to the equation for the total stiffness, the performance of close-to-optimum MR fluid filled spring design can be shown as function of the magnetic field applied (Figure 4.3).

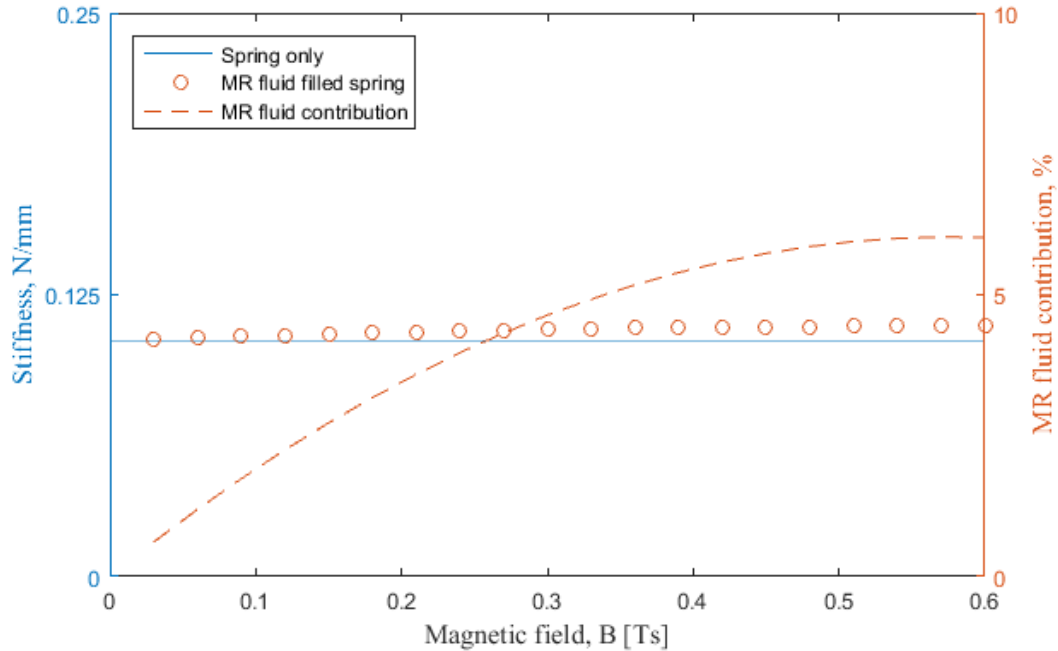


Figure 4.3 Performance of close-to-optimum MR fluid filled spring design ($G = 0.5$ GPa, $\xi = 0.875$, $\alpha = 5^\circ$, $i = 4.5$).

In the Figure 4.3, the curve of MR fluid contribution shows that MR fluid effect can reach up to around 6% of the overall stiffness for springs made of materials with low shear modulus (different types of polymers) with sufficient values of the magnetic field. The MR fluid effect can be improved by using more advanced MR fluids, which has higher values of complex shear modulus and yield stress. However, the lack of studies on their shear moduli limits the present estimation of MR fluid spring performance. Even for commercial MF fluids entered into the market about 10 years ago, such as MRF-140CG (LORD, 2008), the shear modulus is a poorly studied mechanical property. Apparently, such a disregard of the shear modulus can be explained by sufficiency of other properties, such as yield stress and viscosity, to perform the flow analysis in most of MR fluid applications. In cases of MR dampers, brakes, clutches etc., the fluid stays in post-yield state and the shear modulus is not required for analysis of these devices.

5. Numerical Approach

To numerically evaluate the MR fluid effects in the hollow spring, the finite element analysis of the MR fluid filled spring is performed by means of 2-way Fluid-Structural Interaction (FSI) in ANSYS, particularly using ANSYS Mechanical and CFX. The goal of the numerical solution is to validate the results obtained by analytical approach and to observe the transient solution of the problem.

5.1 Steady-state simulation

Before analyzing the transient solution, the steady-state simulation is performed to observe the MR fluid effect and compare it to one obtained through the analytical solution. The coupling of the numerical solvers is shown in Figure 5.1.

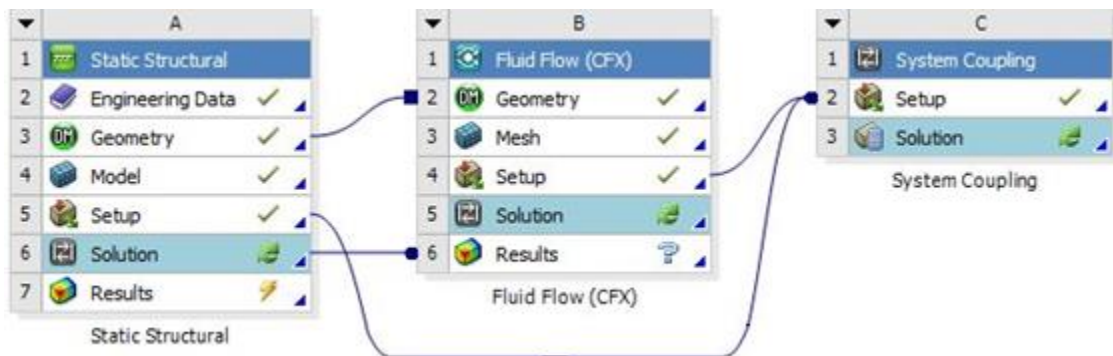


Figure 5.1 Coupling of numerical solver in 2-way steady-state simulation.

The hollow spring is modeled with the geometry parameters shown in Table 5.1.

Table 5.1 Geometry of the helical hollow spring

Number of revolutions (turns)	2.5
Pitch of the spring	12 mm
Mean diameter of the spring	36 mm
Outer radius of the annular cross section	6 mm
Inner radius of the annular cross section	5 mm
Void ratio of the annular cross section	0.833

The small number of spring turns is used to reduce the number of nodes and computational time of numerical solution. The number of spring turns of 2.5 is chosen to reduce the bending and transverse deflections of the spring. Silicon was supposed to be used as the hollow spring material. However, due to low stiffness of the material, high deflection of the spring and corresponding high MR fluid induced viscous forces cause an unstable numerical solution. To simplify the simulation, structural steel is used as the material for the hollow spring in the further simulations. At the meshing step, the default mesh is improved by applying different techniques, while the total number of nodes is kept relatively small. The results of the mesh process in both ANSYS Mechanical and CFX can be seen in Figure 5.2 and Table 5.2.

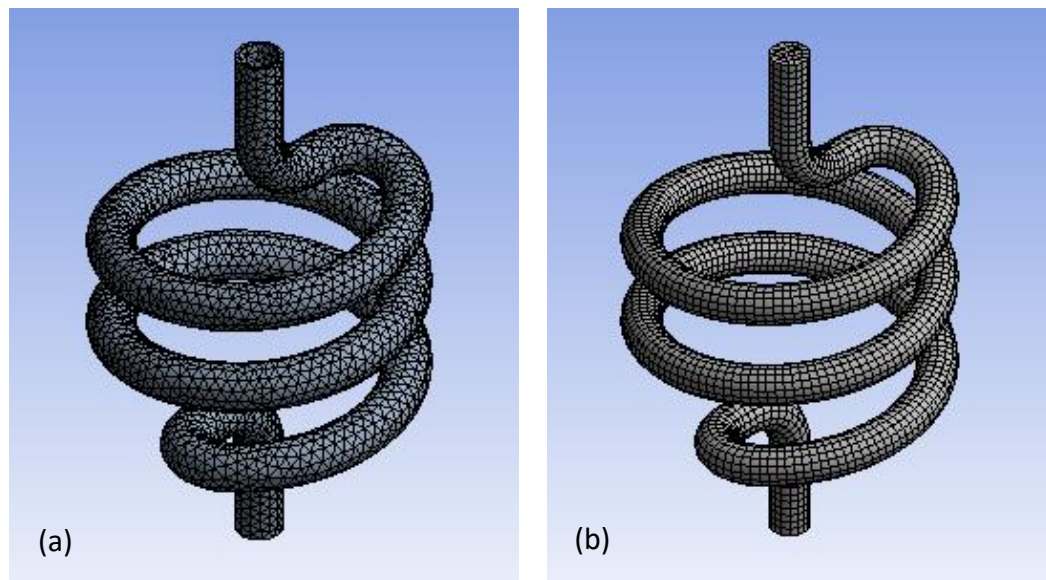


Figure 5.2 Meshes in (a) ANSYS Mechanical and (b) CFX.

In Table 5.2, it can be seen that even the improved mesh is not of very high quality. The poor quality of the mesh is due to the complexity of the geometry, particularly its curvature in both cases and the high surface area-to-volume ratio of the hollow spring.

In CFX, the liquid is modeled as incompressible non-Newtonian fluid using

Bingham viscosity model with yield stress of 50 kPa and viscosity of $0.112 \text{ Pa} \cdot \text{s}$. To stabilize the numerical solution, the axial force is applied gradually to the spring and the MR fluid induced viscous forces are controlled by a mass flux pressure coefficient on the FSI surface as well as an under relaxation factor. The wall boundary condition is used at the top and the bottom of the spring to imitate closed volume of MR fluid inside the spring.

Table 5.2 Mesh quality in ANSYS Mechanical and CFX (Steady-state simulation).

ANSYS Mechanical				
Number of nodes		Element quality	Aspect ratio	Skewness
7223	Min	0.1233	1.380	0.1011
	Max	0.9242	12.69	0.8977
CFX				
Number of nodes		Element quality	Aspect ratio	Skewness
13455	Min	0.4667	1.088	$2.872\text{e-}2$
	Max	0.9880	2.997	0.4084

To evaluate the MR fluid effect, the solution for steady-state 2-way FSI simulation is compared to the steady-state simulation of the hollow spring with the same mesh, boundary conditions, and the 100 N applied load (Figure 5.3).

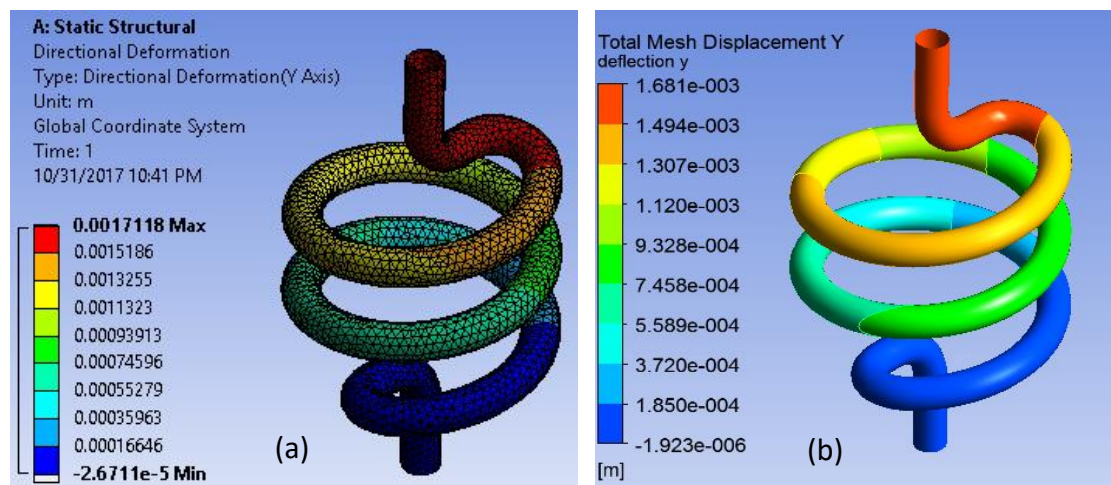


Figure 5.3 Steady-state (a) ANSYS Mechanical and (b) FSI solutions for the deflection of the MR fluid and hollow spring

The comparison shows that the spring filled with MR fluid deflected less than the empty hollow spring, 1.681mm and 1.712mm respectively. The increase in stiffness of the spring is 1.81%; however, it may not be only due to MR fluid effect. The simulation shows some drop of pressure in MR fluid by around 25 kPa averaging throughout the spring, while the reference value is 100 kPa (1 atmosphere). This pressure change in MR fluid is caused by the deformation of the annular cross section of the hollow spring, i.e. change in its inner volume. The pressure change resists the deformation of the hollow spring, and thus, creates an additional stiffness component of MR fluid filled spring. Although the pressure change is small, the MR fluid is modeled as incompressible liquid in CFX, which could constitute a large portion of the resistant force. Hence, compressible fluid model should be used to improve the accuracy of the result.

5.2 Transient simulation

Transient 2-way FSI simulation is performed to account for dynamic loading effect on MR fluid filled spring. The spring geometry, boundary conditions, and load applied are the same as in the steady-state simulation. The mesh applied to the spring in Structural Transient part of the simulation is refined up to about 40,000 nodes, keeping about the same values of mesh quality. That is done as inadequate convergence is observed for Structural part in Steady-state FSI simulation. To achieve a stable numerical solution and its convergence, same techniques as in the steady-state simulation are applied. In addition, the steady-state solution, particularly the mean value of pressure, is used as the initial conditions in CFX part of the transient simulation to start the numerical solver from the point closer to the solution and to get a stable convergence. The time step is required to be small to achieve a reasonable solution; however, it must be maximized to reduce the

computational time, while the mass flux pressure coefficient is tuned to keep an adequate convergence. Nevertheless, the step time is increased only up to $2e-7$ s, which gives 10,000 coupling steps according to the total simulation time. The under relaxation factor is kept to be 1, not to have longer convergence at every iteration step.

First, the transient simulation of hollow spring is performed to observe dynamic response of the current spring design. The amount of time required for the spring to reach its maximum deflection (about 0.002 s) is used as final simulation time for FSI simulation to minimize the computational time (Figure 5.4).

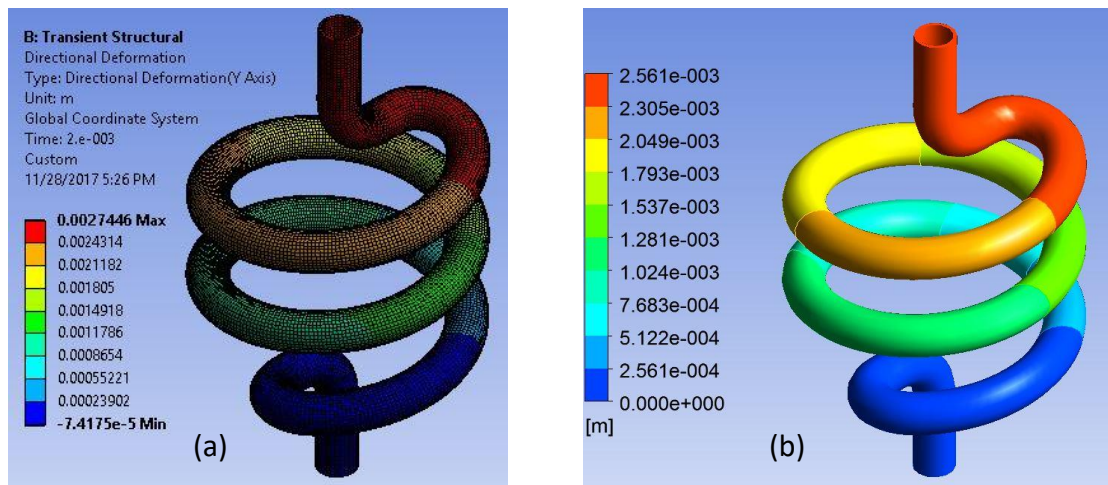


Figure 5.4 Transient (a) ANSYS Mechanical and (b) FSI solutions for the deflection of the MR fluid and hollow spring

The maximum deflection of the MR fluid filled spring is reduced by about 6.7% comparing to the hollow spring. The pressure change is also larger than it is observed in Steady-state FSI simulation, having both low- and high-pressure areas ranging from -58.6 to +49.3 kPa with the reference pressure value of 100 kPa (1 atmosphere). It is observed that variation of MR fluid viscosity significantly influence the pressure change in the liquid. Hence, it might be used to highly increase the amount of controllable stiffness in case of dynamic loading of the MR fluid filled spring.

6. Conclusions

The effect of MR fluid on the stiffness of hollow mechanical spring is analytically studied with some assumptions made numerically. The viscous portion of MR fluid stiffness is proven to be negligibly small for the particular application. The accuracy of the equations is validated by comparing the analytical solutions to known experimental work, showing small difference between both results. The analytical solution calculated in this paper shows that the controllable stiffness by activating MR fluid in the hollow spring is appeared to be relatively small. Sufficient change in stiffness can be achieved only for the spring made of compliant materials and/or ones having large void ratios. However, it might be significantly increased by using more advanced existing MR fluids the shear moduli of which are not studied.

2-way FSI simulation is performed to prove the effect of MR fluid on the spring. It is observed that there is an additional component of resistant force due to pressure change, which depends on the value of MR fluid viscosity. Hence, the controllable MR fluid effect can be increased.

To estimate the pressure component more precisely, compressible fluid model must be implemented in the FSI simulation. The deformation of the spring cross section and compressibility of MR fluid must be considered in analytical analysis to account for the effect of the pressure change. The FSI simulation of the silicone spring filled with MR fluid is to be performed to be able to compare its results with the experimental data of the previous study on MR fluid filled spring and the analytical solution of the present work.

REFERENCES

- Ahmadkhanlou, F., Mahboob, M., Bechtel, S., & Washington, G. (2010). An Improved Model for Magnetorheological Fluid-Based Actuators and Sensors. *Journal of Intelligent Material Systems and Structures* 21.
- Akai, K., Bray, J. D., Boulanger, R. W., et al. (1995). Geotechnical reconnaissance of the effects of the January 17, 1995, Hyogoken-Nanbu earthquake, Japan. *Earthquake Engineering Research Center, College of Engineerins, University of California at Berkley.*
- An, J., & Kwon, D. S. (2003). Modeling of a Magnetorheological Actuator Including Magnetic Hysteresis. *Journal of Intelligent Material Systems and Structures* 14 (9): 541-550.
- Ardelean, E. V., McEver, M. A., Cole, D. G., & Clark, R. L. (2006). Active flutter control with V-stack piezoelectrical flap actuator. *Journal of Aircraft* 15: 482-486
- Ashtiani, M., Hashemabadi, S. H., & Ghaffari, A. (2014). A review on the magnetorheological fluid preparation and stabilization. *Journal of Magnetism and Magnetic Materials* 374: 716-730.
- Austruy, J. (2011). Rotor Hub Vibration and Blade Loads Reduction, and Energy Harvesting via Embedded Radial Oscillator. Dissertation, Department of Aerospace Engineering, The Pennsylvania State University.
- Bertotti, G. (1998). *Hysteresis in Magnetism for Physicists, Material Scientists, and Engineers.* Academic Press.
- BWI Group. Magneride Controlled Suspension System, [Online]. Available: <http://www.bwigroup.com/product/magneride-controlled-suspension-system> [Accessed: October 16th, 2017].
- BWI Group. Magneto-Rheological Powertrain Mounts, [Online]. Available: <http://www.bwigroup.com/product/magneto-rheological-powertrain-mounts> [Accessed: October 16th, 2017].
- Carlson, D., Marjoram, B., Toscano, J., Leroy, D., Burson, K., St Clair, K., Kintz, A., & Achen, A. (2007). *Magneto-rheological Technology and Aplications.* LORD Corporation.
- Carlson, J. D., & Jolly, M. R. (2000). MR fluid, foam and elastomer devices. *Mechatronics* 10: 555-569.
- Carlson, J. D., Matthis, W., Toscano, J. R., & Motech, B. (2001). Smart Prosthetics Based On Magnetorheological Fluids. *Proceedings of SPIE* 4332.

- Chiu, Y., & Hsu, S. (2013). "Taipower says it will fix broken turbine". Taipei Times, [online]. Available: <http://www.taipeitimes.com/News/taiwan/archives/2013/07/08/2003566614> [Accessed: October 27th, 2017].
- Choi, S. B., & Han, Y. M. (2013). Magnetorheological fluid technology: application in vehicle systems. CRC Press.
- Choi, S. B., Hong, S. R., Sung, K. G., & Sohn, J. W. (2008). Optimal control of structural vibrations using a mixed-mode magnetorheological fluid mount. *International Journal of Mechanical Science* 50: 559-568.
- Choi, Y. T., & Wereley, M. N. (2003). Vibration Control of a Landing Gear System Featuring Electrorheological/ Magnetorheological Fluid. *Journal of Aircraft* 40 (3): 432-439.
- Chu, S. Y., Soong, T. T., & Reinhorn, A. M. (2005). Active, hybrid, and semi-active structural control: a design and implementation handbook. John Wiley & Sons, Ltd.
- Ciocanel, C. (2006). A Particle Based Constitutive Model for MR (Magnetorheological) Fluids. Dissertation, College of Engineering, The University of Toledo.
- Ciupitu, L., & Simionescu, I. (2014). Optimum Design of Balancing Systems with Cylindrical Helical Extension Springs. *Applied Mechanics and Materials* 656: 232-241.
- Coleman, B. D., & Hodgdon, M. L. (1986). A constitutive Relation for Rate-Independent Hysteresis in Ferro-magnetically Soft materials. *International Journal of Engineering Science* 24 (6).
- Damanpack, A. R., Bodaghi, M., Aghdam, M. M., & Shakeri, M. (2014). On the vibration control capability of shape memory alloy composite beams. *Composite Structures* 110.
- FAA (1965). 14 CFR Part 25: Airworthiness Standards: Transport Category Airplanes. Federal Aviation Administration.
- Fakhreddine, D., Mohamed T., Said, A., Abderrazek, D., & Mohamed, H. (2005). Finite element method for stress analysis of isotropic cylindrical helical spring. *European Journal of Mechanics, A/Solids* 24: 1068-1078.
- Forte, P., Paterno, M., & Rustighi, E. (2004). A Magnetorheological Fluid Damper for Rotor Applications. *International Journal of Rotating Machinery* 10 (3).
- Gere, J. M., & Timoshenko, S. P. (1991). *Mechanics of Materials*. Nelson Thornes Ltd, Cheltenham, Great Britain.

- Goncalves, D. F. (2005). Characterizing the Behavior of Magnetorheological Fluids at High Velocities and High Shear Rates. Dissertation, Department of Mechanical Engineering, Virginia Polytechnic Institute and State University, Blacksburg, Virginia.
- Goncalves, F. D. (2005). Characterizing the Behavior of Magnetorheological Fluids at High Velocities and High Shear Rates. Dissertation, Department of Mechanical Engineering, Virginia Polytechnic institute and State University.
- Gregory, J. H., Hu, W., & Wereley, N. M. (2008). Semi-active Magnetorheological Helicopter Crew Seat Suspension for Vibration Isolation. *Journal of Aircraft* 45 (3).
- Grover, H. J. (1966). *Fatigue of Aircraft Structures*. Naval Air Systems Command Department of the Navy.
- Guo, S., Yang, S., & Pan, C. (2006). Dynamic Modeling of Magnetorheological Damper Behaviors. *Journal of Intelligent Materials Systems and Structures* 17.
- Hiemenz, J. G. (2007). Semi-Active Magnetorheological Seat Suspension for Enhanced Crashworthiness and Vibration Isolation of Rotorcraft Seats. Dissertation, Department of Aerospace Engineering, University of Maryland, College Park.
- Hodges, D. H., & Pierce, G. A. (2011). *Introduction to Structural Dynamics and Aeroelasticity*. Cambridge University Press.
- IIT Kanpur (2009). Fluid Mechanics, Chapter 8, Lecture 26, [Online]. Available: http://nptel.ac.in/courses/112104118/lecture-26/26-6_concentric_rotate.htm [Accessed: November 30th, 2016].
- Jolly, M. R., Bender, J. W., & Carlson, J. D. (1999). Properties and Applications of Commercial Magnetorheological Fluids. *Journal of Intelligent Material Systems and Structures* 10 (1): 5-13.
- Kamath, G. M., Wereley, N. M., & Jolly, M. R. (1999). Characterization of Magnetorheological Helicopter Lag Dampers. *Journal of the American Helicopter Society* 44 (3): 234-248.
- Laun, H. M., Gabriel, C., & Kieburg, C. (2010). Magnetorheological Fluid in Oscillatory Shear and Parameterization with Regard to MR Device Properties. *Journal of Intelligent Material Systems and Structures* 21: 1479-1489.
- LORD Corporation (2009). LORD TFD Steer-By-Wire Device. Available: http://lordfulfillment.com/pdf/44/PB8130_TFDBrochure.pdf [Accessed: October 16th, 2017].

- LORD Corporation (2011). MRF-132DG Magneto-Rheological Fluid, [Online]. Available: http://ww2.lord.com/Documents/Distributor%20Data/DS7015_MRF-132DGMRFfluid.pdf [Accessed: November 30th, 2016].
- LORD Corporation (2008). MRF-140CG Magneto-Rheological Fluid, [Online]. Available: <http://www.lordfulfillment.com/upload/DS7012.pdf> [Accessed: November 31th, 2017]
- LORD Corporation (2011). Vibration, Shock & Motion Control Products: For Sensitive Equipment, Shipping Containers & Aircraft Interiors.
- LORD Corporation. Industrial Suspension Systems, [Online]. Available: <https://www.lord.com/products-and-solutions/active-vibration-control/industrial-suspension-systems> [Accessed: October 16th, 2017].
- LORD Corporation. Steering Units, [Online]. Available: <https://www.lord.com/products-and-solutions/steering-units> [Accessed: October 16th, 2017].
- Love, A. E. H. (1927). A Treatise on the Mathematical Theory of Elasticity. Cambridge University Press, London.
- MW Industries inc. (2016). Titanium Springs [Online]. Available: <https://www.mw-ind.com/product-types/titanium-springs> [Accessed: October 30th, 2017].
- Naji, J., Zabihollah, A., & Behzad, M. (2016). Layerwise theory in modelling of magnetorheological laminated beams and identification of magnetorheological fluid. *Mechanics Research Communications* 77: 50-59.
- Ngatu, T. G., Hu, W., Wereley, M. N., & Kothera, S. C. (2010). Adaptive Snubber-Type Magnetorheological Fluid-Elastomeric Helicopter Lag Damper. *AIAA Journal* 48 (3): 598-610.
- Ohanian, H. C., & Markert, J. T. (2007). *Physics, for Engineers and Scientists*, volume 1, 3rd ed., W.W. Norton & Co.
- Onoda, J., Oh, H. U., & Minesugi, K. (1997). Semi-active Vibration Suppression with Electrorheological-Fluid Damper. *AIAA Journal* 35 (12).
- Poynor, J. C. (2001). Innovative designs for magneto-rheological dampers. Thesis, Department of Mechanical Engineering, Virginia Polytechnic Institute and State University.
- Prakash, S., Venkatasubramanyam, D. V., Krishnan, B., Pavate, A., & Kabra, H. (2009). Active Vibration Control of a Composite Wind Model using PZT Sensors/Actuators & Virtex – 4 FPGAs. *Proceedings of SPIE* 7493 (1).

- Pramanik, S. (2014). Casson fluid flow and heat transfer past an exponentially porous stretching surface in presence of thermal radiation. *Ain Shams Engineering Journal* 5: 205-212.
- Premalatha, S. E., Chokkalingam, R., & Mahendran, M. (2012). Magneto Mechanical Properties of Iron Based MR Fluids. *American Journal of Polymer Science* 2 (4): 50-55.
- Preumont, A. (2011). *Vibration control of active structures*, 3rd ed., Springer, Berlin.
- Punmia, B. C., Jain, A. K., & Jain, A. K. (2002). *Mechanics of Materials*. Laxmi Publications (P) Ltd., New Delhi.
- Rajamohan, V. (2010). *Vibration analysis and optimization of fully and partially MR-fluid treated multi-layer beam*. Dissertation, Department of Mechanical and Industrial Engineering, Concordia University, Montreal, Quebec, Canada.
- Rajamohan, V., Rakheja, S., & Sedaghati, R. (2010). Vibration analysis of a partially treated multi-layer beam with magnetorheological fluid. *Journal of Sound and Vibration* 329: 3451-3469.
- Reddy, P. B. A. (2016). Magneto hydrodynamic flow of a Casson fluid over an exponentially inclined permeable stretching surface with thermal radiation and chemical reaction. *Ain Shams Engineering Journal* 7: 539-602.
- Richardson, M. H., & Ramsey K. A. (1981). Integration of dynamic testing into the product design cycle. *Sound and Vibration* 15 (11): 14-27.
- Rodriguez-Lopez, J., Castro, P., Vicente, J., Johannsmann, D., Elvira, L., Morillas, J. R., & Espinosa, F. M. (2015). Colloidal Stability and Magnetic Field-Induced Ordering of Magnetorheological Fluids Studied with a Quartz Crystal Microbalance. *Sensors* 15: 30443-30456.
- Shmyrov, V. F., Tsukanov, R. U., Ryzhenko, A. I., & Pehterev, V. D. (2010). *Airplane Power Plants Systems Designing*. National Aerospace University "KhAI".
- Sidpara, A., Das, M., & Jain, V.K. (2009). Rheological Characterization of Magnetorheological Finishing Fluid. *Materials and Manufacturing Processes* 24: 1467-1478.
- Simon, T.M., Reitich, F., Jolly, M. R., Ito, K., & Banks, H. T. (2001). The Effective Magnetic Properties of Magnetorheological Fluids. *Mathematical and Computer Modelling* 33: 273-284.

- Spaggiari, A. (2013). Properties and applications of Magnetorheological fluids. *Frattura ed Integrità Strutturale* 23: 57-61.
- Spelta, C., Previdi, F., Savaresi, S. M., Fraternali, G., & Gaudiano, N. (2009). Control of magnetorheological dampers for vibration reduction in a washing machine. *Mechatronics* 19: 410-421.
- Spinella, I., & Dragoni, I. (2010). Analysis and Design of Hollow Helical Springs for Shape Memory Actuators. *Journal of Intelligent Material Systems and Structures* 21: 185-199.
- Sun, Q., Zhou, J., & Zhang, L. (2003). An adaptive beam model and dynamic characteristics magnetorheological materials. *Journal of Sound and Vibration* 261: 465-481.
- Suresh, K., Park, C. Y., & Choi, S. B. (2015). Bio-inspired device: a novel smart MR spring featuring tendril structure. *IOP Publishing* 25 (1).
- Tang, X., Zhang, X., & Tao, R. (2000). Structure-Enhanced Yield Stress of Magnetorheological Fluids. *Journal of Applied Physics* 87 (5).
- Thakkar, R. M., Shah, D. R., & Modan, M. Y. M. (2013). Modeling and Simulation of Magnetorheological Fluid Damper for Predicting the Saturation Limit to Applied Field Current. *Global Journal for Research Analysis* 2 (3): 69-71.
- Transportation Safety Board of Canada (2007). Aviation Investigation Report A05F0047, Loss of Rudder in Flight, Air Transat, Airbus A310-308 C-GPAT. Minister of Public Works and Government Services Canada.
- Vignesh, M. (2016). Magneto-Rheological Fluid Device as Artificial Feel Force System on Aircraft Control Stick. Thesis, Department of Aerospace Engineering, Embry-Riddle Aeronautical University.
- Wahl, A. M. (1944). *Mechanical Springs*, 1st ed. Penton Publishing Company, Cleveland.
- Walid, H. A. (2002). Finite Element Analysis Based Modeling of Magneto Rheological Dampers. Thesis, Department of Mechanical Engineering, Virginia Polytechnic Institute and State University, Blacksburg, Virginia.
- Wang, C. Y., & Wang C. M. (2014). *Structural Vibration: Exact Solution for Spring, Membranes, Beams, and Plates*. Taylor & Francis Group.
- Wang, H., Zheng, H., Li, Y., & Lu, S. (2008). Mechanical properties of magnetorheological fluids under squeeze-shear mode. *Proceedings of SPIE* 7130.

- Wang, J., & Meng, G. (2001). Magnetorheological fluid devices: principles, characteristics and applications in mechanical engineering. *Proceedings of the Institution of Mechanical Engineers, Part L: Journal of Materials: Design and Applications* 215: 165-174.
- Xu, Z. D., Guo, Y. Q., Zhu, J. T., Xu, F. H., & Xu, F. H. (2016). *Intelligent Vibration Control in Civil Engineering Structures*. Elsevier Science.
- Yang, G., Spencer, B. F., Carlson, J. D., & Sain, M. K. (2002). Large-scale MR fluid dampers: modeling and dynamic performance considerations. *Engineering Structures* 24: 309-323.
- Yang, J., Yan, H., Wang, X., & Hu, Z. (2015). Enhanced yield stress of magnetorheological fluids with dimer acid. *Materials Letters* 167: 27-29.
- Yao, G. Z., Yap, F. F., Chen, G., Li, W. H., & Yeo, S. H. (2002). MR damper and its application for semi-active control of vehicle suspension system. *Mechatronics* 12 (7): 963-973.
- Yildirim, V. (2016). Exact determination of the global tip deflection of both close-coiled and open-coiled cylindrical helical compression springs having arbitrary doubly-symmetric cross-sections. *International Journal of Mechanical Sciences* 115-116: 280-298.
- Zhu, X., Jing, X., & Cheng, L. (2012). Magnetorheological fluid damper: A review on structure design and analysis. *Journal of Intelligent Material Systems and Structures* 23 (8): 839-873.